Indirect constraints on top quark operators from a global SMEFT analysis

Francesco Garosi,[a,b] **David Marzocca,**[b] **Antonio Rodríguez-Sánchez**[a,b]
and Alfredo Stanzione[a,b]

[a]*SISSA International School for Advanced Studies,*
 Via Bonomea 265, 34136, Trieste, Italy

[b]*INFN, Sezione di Trieste, SISSA,*
 Via Bonomea 265, 34136, Trieste, Italy

 E-mail: fgarosi@sissa.it, david.marzocca@ts.infn.it,
 arodrigu@sissa.it, astanzio@sissa.it

ABSTRACT: We perform a model-independent analysis of top-philic New Physics scenarios, under the assumption that only effective operators involving top quarks are generated at tree level. Within the SMEFT framework, we derive indirect constraints on Wilson Coefficients by combining a large set of low-energy observables: B-meson and kaon decays, meson mixing observables, precision electroweak and Higgs measurements, anomalous magnetic moments, lepton flavour violating processes, lepton flavour universality tests, and measurements of the Cabibbo angle. We consider the renormalization group evolution of the operators and use the one-loop matching of the SMEFT onto the LEFT. The global analysis is then used to perform one-parameter, two-parameter, and global fits, as well as applications to explicit ultraviolet models. We find that the inclusion of measurements from different physics sectors reveals a strong interplay and complementarity among the observables. The resulting constraints are also compared to direct bounds provided by top quark productions at the LHC.

Contents

1 Introduction

The top quark plays a special role both in the Standard Model (SM) and beyond, due to its large mass or, in other terms, to its $\mathcal{O}(1)$ Yukawa coupling to the Higgs. In the SM, due to the GIM mechanism [1], it generates the dominant loop contribution in many low-energy flavour-changing neutral-current (FCNC) processes. It also induces some of the leading radiative corrections in the electroweak (EW) sector, it is the main driver of the renormalization group evolution of the quartic Higgs coupling, and it is the main culprit of the (meta-)stability of the Higgs potential. The top quark also generates the largest corrections to the Higgs mass, therefore going beyond the SM it is a crucial actor in all New Physics scenarios that aim at addressing the naturalness problem of the EW scale. For instance, the so-called top partners are expected to be some of the lightest new particles in such scenarios, both in supersymmetric (stops) and in composite Higgs (vectorlike top partners) models. This expectation is reinforced by the fact that experimental constraints from direct searches of these particles are generally weaker than for the partners of the lighter quarks. Furthermore, due to the large top mass, its couplings to EW gauge bosons are still not so strongly constrained and large new physics (NP) effects could still hide there. Therefore, in many NP scenarios the new states couple most strongly to the top quark. See ref. [2] for a recent review.

For all these reasons it is reasonable to assume that NP might be more strongly coupled to the top quark than to the other fermions. If such NP is heavy, then at low energy its effect can be described by effective operators that involve the top quark. In this work we assume that at a UV scale Λ (we fix $\Lambda = 1\,\mathrm{TeV}$ for concreteness) only effective operators involving the top quark are generated at the tree level and we study the indirect constraints that can be obtained on the corresponding coefficients by considering the effects they have on a large set of low energy observables, comparing these to the direct constraints that have been obtained by studying top quark processes at the LHC.

We work in the Standard Model Effective Field Theory (SMEFT) and choose the Warsaw basis [3] of dimension-six operators:[1]

$$\mathcal{L}_{\mathrm{SMEFT}} = \mathcal{L}_{\mathrm{SM}} + \sum_i \frac{c_i^{(6)}}{\Lambda^2} \mathcal{O}_i^{(6)} + \dots . \tag{1.1}$$

As stated above, we focus on top-quark operators, i.e. operators that among quarks involve only the third generation quark doublet q^3 and right-handed top u^3, assuming that all other vanish. The lepton sector is instead left completely general, since we want to consider also tests of lepton flavour universality (LFU) and lepton flavour violation (LFV). The set of SMEFT operators is then reduced to the list in table 1. In the following, the superscripts '3' for quark indices in SMEFT coefficients are omitted, as they are in the table. We work with the rescaled coefficients $C_i \equiv \frac{c_i^{(6)}}{\Lambda^2}$ in TeV^{-2} units.

While in the limit where only the top quark mass is considered the gauge and mass bases are the same, we want to describe also the mixing with light generations via the

---

[1]We assume baryon and lepton number conservation at the scale Λ.

Semi-leptonic		Four quarks	
$\mathcal{O}_{lq}^{(1),\alpha\beta}$	$(\bar{l}^a\gamma_\mu l^\beta)(\bar{q}^3\gamma^\mu q^3)$	$\mathcal{O}_{qq}^{(1)}$	$(\bar{q}^3\gamma^\mu q^3)(\bar{q}^3\gamma_\mu q^3)$
$\mathcal{O}_{lq}^{(3),\alpha\beta}$	$(\bar{l}^a\gamma_\mu\tau^a l^\beta)(\bar{q}^3\gamma^\mu\tau^a q^3)$	$\mathcal{O}_{qq}^{(3)}$	$(\bar{q}^3\gamma^\mu\tau^a q^3)(\bar{q}^3\gamma_\mu\tau^a q^3)$
$\mathcal{O}_{lu}^{\alpha\beta}$	$(\bar{l}^\alpha\gamma^\mu l^\beta)(\bar{u}^3\gamma_\mu u^3)$	$\mathcal{O}_{uu}$	$(\bar{u}^3\gamma^\mu u^3)(\bar{u}^3\gamma_\mu u^3)$
$\mathcal{O}_{qe}^{\alpha\beta}$	$(\bar{q}^3\gamma^\mu q^3)(\bar{e}^\alpha\gamma_\mu e^\beta)$	$\mathcal{O}_{qu}^{(1)}$	$(\bar{q}^3\gamma^\mu q^3)(\bar{u}^3\gamma_\mu u^3)$
$\mathcal{O}_{eu}^{\alpha\beta}$	$(\bar{e}^\alpha\gamma^\mu e^\beta)(\bar{u}^3\gamma_\mu u^3)$	$\mathcal{O}_{qu}^{(8)}$	$(\bar{q}^3\gamma^\mu T^A q^3)(\bar{u}^3\gamma_\mu T^A u^3)$
$\mathcal{O}_{lequ}^{(1),\alpha\beta}$	$(\bar{l}^\alpha e^\beta)\epsilon(\bar{q}^3 u^3)$	Higgs-Top	
$\mathcal{O}_{lequ}^{(3),\alpha\beta}$	$(\bar{l}^\alpha\sigma_{\mu\nu}e^\beta)\epsilon(\bar{q}^3\sigma^{\mu\nu}u^3)$	$\mathcal{O}_{Hq}^{(1)}$	$(H^\dagger i\overleftrightarrow{\mathcal{D}}_\mu H)(\bar{q}^3\gamma^\mu q^3)$
Dipoles		$\mathcal{O}_{Hq}^{(3)}$	$(H^\dagger i\overleftrightarrow{\mathcal{D}}_\mu^a H)(\bar{q}^3\gamma^\mu\tau^a q^3)$
$\mathcal{O}_{uG}$	$(\bar{q}^3\sigma^{\mu\nu}T^A u^3)\tilde{H}G_{\mu\nu}^A$	$\mathcal{O}_{Hu}$	$(H^\dagger i\overleftrightarrow{\mathcal{D}}_\mu H)(\bar{u}^3\gamma^\mu u^3)$
$\mathcal{O}_{uW}$	$(\bar{q}^3\sigma^{\mu\nu}u^3)\tau^a\tilde{H}W_{\mu\nu}^a$	$\mathcal{O}_{uH}$	$(H^\dagger H)(\bar{q}^3 u^3\tilde{H})$
$\mathcal{O}_{uB}$	$(\bar{q}^3\sigma^{\mu\nu}u^3)\tilde{H}B_{\mu\nu}$		

Table 1. The 19 dimension-six operators considered in this work. They can be split in four classes, depending on the fields coupled to the Top quark. We keep the lepton flavour structure arbitrary.

Cabibbo-Kobayashi-Maskawa (CKM) matrix and therefore we must consider all quark masses. In this case, the flavour basis at the scale Λ is in general different than the quark mass bases, forcing us to make a flavour assumption at the high scale. Two common choices in the literature are the up or down quark mass bases. If only the operators listed above are considered, then the results of the fit will of course depend on this choice.[2] Since we are assuming that new physics is mostly coupled to the top quark, it is logical to work in the up-quark and charged-lepton mass basis, where $q^i = (u_L^i, V_{ij}d_L^j)$, $l^\alpha = (\nu_L^\alpha, \ell_L^\alpha)$, and V is the CKM matrix. This will induce CKM-suppressed operators involving first and second generation left-handed down quarks.

We aim at deriving indirect constraints on all these operators by considering a large set of low-energy observables in a global analysis. We include rare B-meson and kaon decays, meson mixing observables, all the processes used to measure the Cabibbo angle, anomalous magnetic moments of the electron and muon, lepton flavour universality tests in charged-current lepton decays, charged lepton flavour-violating processes, and precision electroweak and Higgs measurements. To obtain the dependence of these observables on

---

[2]One alternative could be to introduce a consistent flavour symmetry, for instance $\mathrm{U}(2)_q \times \mathrm{U}(2)_u \times \mathrm{U}(2)_d$ [4–6], and symmetry-breaking spurions, and consider then also the operators suppressed by the spurions, see e.g. ref. [7]. This would however increase greatly the number of coefficients to fit and goes beyond the purpose of our work.

our SMEFT coefficients, we evolve them from the scale Λ down to the low-energy scale relevant for each observable using the renormalization group evolution in the SMEFT and in the low-energy effective field theory (LEFT), including the one-loop matching between the two. Finally, we build a global likelihood and perform several fits on the coefficients of top quark operators.

Several groups studied indirect constraints on top anomalous interactions or top quark operators. Refs. [8–12] analyzed anomalous top couplings to W and Z bosons, and top quark flavour violation, considering rare meson decays and electroweak precision data. Dipole and scalar SMEFT operators with top quarks have been considered in refs. [13, 14], where indirect bounds from $b \to s\gamma$ and electric dipole moments have been derived after the RG evolution down to the low scale. More recently, ref. [15] performed a more global analysis, where several top quark operators have been considered and the indirect constraints from B-meson observables and $Z \to b\bar{b}$ have been derived and compared with direct limits from LHC. In our work we go beyond these previous analyses by considering a much larger set of top quark operators (all the ones that involve top quarks) and by substantially enlarging the scope of the observables considered.

The paper is structured as follows. In section 2 we present the setup of our analysis, describing in general terms how we build the global likelihood. Section 3 contains an overview of all the observables we take into account, divided into different classes. In section 4 we employ the global likelihood to derive fits in some simplified scenarios and discuss the results: one coefficient at a time, interesting pairs of coefficients, and a Gaussian fit with all coefficients except those of semileptonic operators. To showcase some other applications of our analysis, in section 5 we study two specific UV models that we match to the SMEFT. The first contains a scalar leptoquark coupled only to the third generation quark and lepton doublets. The second simplified model, inspired by the Cabibbo anomaly, contains a scalar and a vector leptoquark. Finally, we conclude in section 6. Appendix A contains details on all the observables included in our analysis.

2 Methodology

Our goal is to constrain TeV-scale top-philic scenarios deriving bounds from a large set of low-energy observables. The EFT approach represents a suitable framework for this task, as it allows us to consistently study and keep track of the scale dependence of the operators in a multi-step procedure. In practice, RGEs connect different energy scales within the range of validity of the EFT, while matching procedures allow us to integrate out heavy degrees of freedom, linking EFTs valid above or below the threshold.

The description of low energy observables below the electroweak scale relies on the LEFT Lagrangian defined in ref. [16]:

$$\mathcal{L}_{\text{LEFT}} = \mathcal{L}_{\text{QED+QCD}} + \sum_i L_i^{(5)} O_i^{(5)} + \sum_i L_i^{(6)} O_i^{(6)} , \qquad (2.1)$$

where the Higgs, W and Z bosons and the top quark have been integrated out, leaving the QCD sector with only two up-type quarks. Higher-dimension non-renormalizable operators
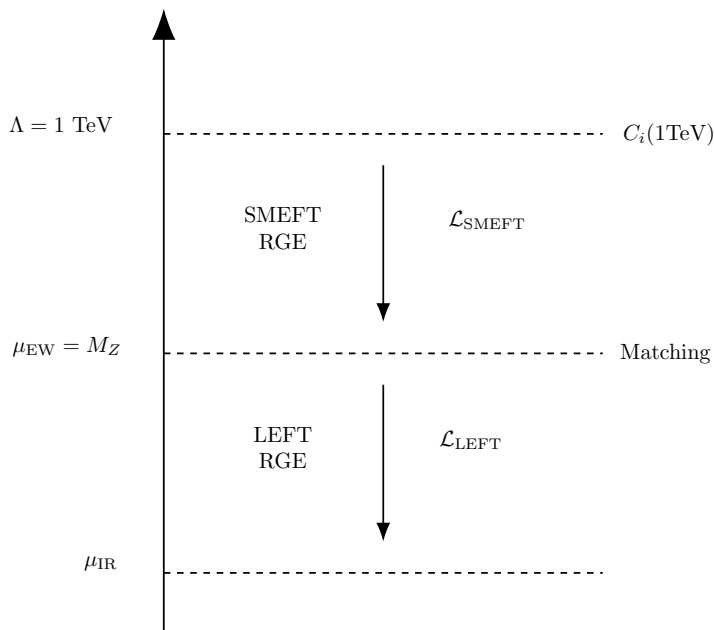
Figure 1. Sketch of the EFT analysis procedure adopted in this work. $\mu_{\rm IR}$ is the scale relevant to the low energy observable under consideration.

are generated both by the SM heavy particles and by SMEFT contributions, again in a model-independent EFT framework. The complete list of LEFT operators is provided in table 15.

After having defined our set of top-quark operators at the UV scale $\Lambda = 1\,{\rm TeV}$, as in eq. (1.1), the matching to the whole set of observables is done through the following steps.

- We evolve the SMEFT coefficients C_i from Λ down to the electroweak matching scale, that we fix to $\mu_{\rm EW} = M_Z \simeq 91.2\,{\rm GeV}$. We perform this running procedure numerically using the DSixTools package [17, 18], which implements the RG equations provided in [19–21].

- As discussed in ref. [22], we combine the one-loop matching with one-loop RG evolution. For the matching between the SMEFT and the LEFT we use the results computed in ref. [23] and refer to its ancillary files for the complete expressions (see also ref. [24]).

- The LEFT coefficients [25] are then evolved from the electroweak scale down to the energy scales $\mu_{\rm IR}$ relevant to the specific experiment, e.g. $\mu_{\rm IR} = 4.2\,{\rm GeV}$ for B decays, again using the DSixTools numerical routines.

- We express the low-energy observables in terms of the LEFT Wilson coefficients generated by the previous steps.

The whole process is sketched in figure 1, where the main steps and the corresponding energy scales are outlined. QCD effects are known to be relevant, especially at low energies,

and a resummation beyond the leading order is required. So, as an exception, we use the five-loop QCD correction for quark Yukawas and the gauge coupling from refs. [26–28] and the four-loop strong coupling beta function and quark mass anomalous dimension from ref. [29]. These QCD corrections are implemented in DSixTools as well as the three-loop SM RGEs from refs. [30–33].

The procedure depicted in figure 1 does not apply to the observables defined above/at the EW scale, when running the SMEFT coefficients up to $\Lambda_{\rm UV}$ is the only necessary step. In some cases, previous studies and results in the literature allowed us to partially or completely skip some steps. These cases will be mentioned and discussed in the following.

Once we have expressed the low energy observables and pseudo-observables in terms of SMEFT Wilson coefficients, we can build the log-likelihood:

$$-2\log\mathcal{L}(C_k) \equiv \chi^2(C_k) = \sum_{i,j}(\mathcal{O}_i(C_k) - \mu_i)\,(\sigma^2)_{ij}^{-1}\,(\mathcal{O}_j(C_k) - \mu_j)\,, \qquad (2.2)$$

where $\mathcal{O}_i$ are the observables, C_k are the Wilson coefficients defined at the TeV scale, μ_i are the experimental values and $(\sigma^2)_{ij}^{-1}$ the corresponding covariance matrix. The likelihood is maximized by looking at the minimum of the chi-square, χ_0^2, so that the quantity $\Delta\chi^2 = \chi^2 - \chi_0^2$ allows to define the 68% or 95% CL regions. We use our global likelihood to perform individual, pairwise and global fits on Wilson coefficients. In practice, we allow only one, two or a subset of parameters in the global $\chi^2(C_i)$ to vary and set to zero all the remaining ones. Results and applications are discussed in sections 4 and 5.

3 Observables

The up quark basis we employ for the left-handed quark doublet makes several top quark operators, such as the ones from table 1, contribute to FCNC $d_L^i \to d_L^j$ transitions even at tree-level, only suppressed by $V_{tj}^* V_{ti}$ factors. Very strong bounds to such BSM contributions can be obtained from rare B and K decays as well as meson mixing observables. Operators with top quarks are also expected to give relevant contributions, via loop effects, to anomalous magnetic moments of leptons, tau decays, electroweak precision data, Higgs measurements and precision measurements entering in Cabibbo-angle analyses. Finally, operators that violate lepton flavour are constrained by LFV tests in lepton and meson decays. In the following subsections we provide some more details on these observables, postponing more detailed discussions to appendix A.

3.1 B physics

SM-suppressed FCNC $b \to s$ transitions are powerful channels to probe new physics, in particular in those observables for which the SM prediction is free from poorly-known long-distance QCD effects. Among these, after the recent update by LHCb [34], the lepton flavour universality (LFU) ratios R_K and R_{K^*} provide stringent constraints on NP coupled to light leptons:

$$\begin{aligned} R_K[1.1, 6] &= 0.949 \pm 0.047\,, \\ R_{K^*}[1.1, 6] &= 1.027 \pm 0.077\,. \end{aligned} \qquad (3.1)$$

Other powerful decay channels for testing new physics are the so-called *golden-channel* decays, for which it can be useful to define the ratios with the SM predictions as

$$R^\nu_{K^{(*)}} \equiv \frac{\mathcal{B}(B \to K^{(*)}\nu\bar{\nu})}{\mathcal{B}(B \to K^{(*)}\nu\bar{\nu})_{\text{SM}}}\,, \qquad (3.2)$$

using the updated SM predictions from ref. [35]. Notably, the Belle-II experiment recently presented the first evidence for a signal in the $B^+ \to K^+\nu\bar{\nu}$ channel: $\mathcal{B}(B^+ \to K^+\nu\bar{\nu})_{\text{Belle-II}} = (2.4 \pm 0.5^{+0.5}_{-0.4}) \times 10^{-5}$ [36]. Once combined with previous upper limits, this becomes $\mathcal{B}(B^+ \to K^+\nu\bar{\nu})_{\text{Comb.}} = (1.4 \pm 0.4) \times 10^{-5}$, to be compared with the SM prediction, $\mathcal{B}(B^+ \to K^+\nu\bar{\nu})_{\text{SM}} = (0.506 \pm 0.031) \times 10^{-5}$. The corresponding value for R^ν_K is reported in table 2. On the other hand, the strongest upper limit on the K^* mode comes from Belle, with $R^\nu_{K^*} < 3.21$ at 95%CL [37] after combining the different modes. Several NP models affect these decay modes as a rescaling of the SM short-distance amplitude, that involves only $V - A$ currents, in such a way that $R^\nu_K = R^\nu_{K^*}$. In this case it is interesting to combine the two modes, obtaining:

$$R^\nu_{K^{(*)}} = 2.23 \pm 0.71\,, \qquad (3.3)$$

compatible with the SM value of 1 at 1.7σ. We emphasize that, since we are not assuming lepton flavour number conservation, the inclusive sum on neutrino final states takes into account LFV cases:

$$\mathcal{B}(B \to K^{(*)}\nu\bar{\nu}) = \sum_{\alpha,\beta=1}^{3} \mathcal{B}(B \to K^{(*)}\nu_\alpha\bar{\nu}_\beta)\,. \qquad (3.4)$$

We conclude the list of B decays by including $B_s \to X_s\gamma$, the leptonic $B_s \to \ell_\alpha\ell_\beta$ decays as well as semileptonic and leptonic LFV modes. The complete list of B-physics observables we consider is displayed table 2, together with measurements provided by the LHCb, Belle(-II) and BaBar experiments.

Theoretical predictions are extensively discussed in appendix A, where branching ratios expressed in terms of low energy EFT coefficients are given. Here, we limit ourselves to show, in table 3, a comprehensive sketch of SMEFT contributions to the observables considered in the work. We briefly discuss WC's relevance and interplay in the rest of this section.

The semileptonic C_{qe} and the combination $(C^{(1)}_{lq} + C^{(3)}_{lq})$ contribute at tree level to $b(d) \to s\ell_\alpha\ell_\beta$ processes, getting constrained by both rare meson $B_{s,d} \to \ell_\alpha\ell_\beta$ and semileptonic $B \to K\ell_\alpha\ell_\beta$ decays. Within these cases, the recent analysis of $R_{K^{(*)}}$ provides strong constraints on light lepton operators (see discussion in section 4.2 and figures therein) up to the $|C_i| \leq 10^{-2}\,\text{TeV}^{-2}$ level. These bounds on semileptonic current-current operators are completed and complemented by dineutrino modes $B \to K\nu\bar{\nu}$, which are sensitive at tree level to the combination $(C^{(1)}_{lq} - C^{(3)}_{lq})$ and to the Higgs-top operators $C^{(1)}_{Hq}$ and $C^{(3)}_{Hq}$.

In general, contributions from 4-quark operators arise in radiative corrections, from both the one-loop matching and the RG evolution. Similarly, the up-type dipole operators C_{uG}, C_{uB} and C_{uW} enter the one-loop matching expression for down-type dipoles,

Observable	Experimental value
$B \to X_s \gamma$	$(3.49 \pm 0.19) \times 10^{-4}$ [38]
R_K^ν	2.77 ± 0.79 [35, 36]
R_{K*}^ν	3.21 [35, 37]
$R_K[1.1, 6]$	0.949 ± 0.047 [34]
$R_{K*}[1.1, 6]$	1.027 ± 0.077 [34]
$\mathcal{B}(B \to K e\mu)$	$< 4.5 \times 10^{-8}$ [39]
$\mathcal{B}(B \to K e\tau)$	$< 3.6 \times 10^{-5}$ [40]
$\mathcal{B}(B \to K \mu\tau)$	$< 4.5 \times 10^{-5}$ [41]

Observable	Experimental value
$\mathcal{B}(B_s \to ee)$	$< 11.2 \times 10^{-9}$ [42]
$\mathcal{B}(B_s \to \mu\mu)$	$(3.01 \pm 0.35) \times 10^{-9}$ [43]
$\mathcal{B}(B_s \to \tau\tau)$	$< 6.8 \times 10^{-3}$ [44]
$\mathcal{B}(B_s \to e\mu)$	$< 6.3 \times 10^{-9}$ [45]
$\mathcal{B}(B_s \to \mu\tau)$	$< 4.2 \times 10^{-5}$ [46]
$\mathcal{B}(B_d \to ee)$	$< 3.0 \times 10^{-9}$ [42]
$\mathcal{B}(B_d \to \mu\mu)$	$< 2.6 \times 10^{-10}$ [43]
$\mathcal{B}(B_d \to \tau\tau)$	$< 2.1 \times 10^{-3}$ [44]
$\mathcal{B}(B_d \to e\mu)$	$< 1.3 \times 10^{-9}$ [45]
$\mathcal{B}(B_d \to \mu\tau)$	$< 1.4 \times 10^{-5}$ [46]

Table 2. Experimental values for B-physics observables included in this work. Bounds are given at 95% CL. In the last column, prospects of future precision are included.

	Tree level matching	RG and 1-loop matching
$B \to X_s \gamma$		$C_{Hq}^{(1,3)}$, C_{uB}, C_{uW}, C_{uG}
$R_{K^{(*)}}^\nu$ $K \to \pi \nu\bar{\nu}$	$C_{Hq}^{(1,3)}$, $C_{lq}^{(1,3),\alpha\beta}$	C_{Hu}, $C_{qq}^{(1,3)}$, $C_{lu}^{\alpha\beta}$, $C_{qe}^{\alpha\beta}$ $C_{qu}^{(1,8)}$, C_{uu}, C_{uW}
$B \to K^{(*)} \ell_\alpha \ell_\beta$ $B_{s,d} \to \ell_\alpha \ell_\beta$ $K \to \pi \ell_\alpha \ell_\beta$ $K \to \ell_\alpha \ell_\beta$	$C_{lq}^{(1,3),\alpha\beta}$, $C_{qe}^{\alpha\beta}$	$C_{lu}^{\alpha\beta}$, $C_{eu}^{\alpha\beta}$, $C_{Hq}^{(1,3)}$
$R_{K^{(*)}}$	$C_{lq}^{(1,3),\ell\ell}$, $C_{qe}^{\ell\ell}$	$C_{lu}^{\ell\ell}$

Table 3. Most relevant WC to B-physics observables. The operators that contribute at tree level are displayed in the left column, while operators generated by radiative corrections are listed in the right column. The indices take values $\alpha, \beta = 1,2,3$ and $\ell = e, \mu$. Transpose conjugate operators are not listed since related to the already mentioned ones, e.g. $C_{lq}^{(1),\beta\alpha} = C_{lq}^{(1),\alpha\beta *}$.

contributing then to the $B \to X_s \gamma$ decays. Inclusive radiative decays and rare $B \to \ell_\alpha \ell_\beta$ decays also constrain the $C_{Hq}^{(1/3)}$ coefficients, making B physics bounds almost comparable to the EW precision tests (see figure (4)).

Remarkably, the lack of direct limits on semileptonic dimension-six operators from top-quark measurements, such as inclusive $t\bar{t}$ and single top productions, makes indirect bounds from B mesons crucial in interpreting top-philic NP scenarios. At the same time, these flavour observables provide competitive or stronger constraints on 4-quark and Higgs-top operators, testing the robustness of global fits.

Observable	Experimental value
$\mathcal{B}(K^+ \to \pi^+ \nu\bar{\nu})$	$(1.14^{+0.4}_{-0.33}) \times 10^{-10}$ [47, 48]
$\mathcal{B}(K_L \to \pi^0 \nu\bar{\nu})$	$< 3.6 \times 10^{-9}$ [49]
$\mathcal{B}(K_S \to \mu^+ \mu^-)$	$< 2.5 \times 10^{-10}$ [50]
$\mathcal{B}(K_L \to \mu^+ \mu^-)_{SD}$	$< 2.5 \times 10^{-9}$ [51]
$\mathcal{B}(K_L \to \mu^\pm e^\mp)$	$< 5.6 \times 10^{-12}$ [52]
$\mathcal{B}(K_L \to \pi^0 \mu^+ \mu^-)$	$< 4.5 \times 10^{-10}$ [53]
$\mathcal{B}(K_L \to \pi^0 e^+ e^-)$	$< 3.3 \times 10^{-10}$ [54]
$\mathcal{B}(K_L \to \pi^0 e^+ \mu^-)$	$< 9.1 \times 10^{-11}$ [55]
$\mathcal{B}(K^+ \to \pi^+ e^+ \mu^-)$	$< 7.9 \times 10^{-11}$ [56]

Table 4. Experimental values for kaon physics observables included in this work. Bounds are given at 95% CL.

Observable	Experimental value	SM prediction
ϵ_K	$(2.228 \pm 0.011) \times 10^{-3}$	$(2.14 \pm 0.12) \times 10^{-3}$
ΔM_s	$(17.765 \pm 0.006)\,\mathrm{ps}^{-1}$	$(17.35 \pm 0.94)\,\mathrm{ps}^{-1}$
ΔM_d	$(0.5065 \pm 0.0019)\,\mathrm{ps}^{-1}$	$(0.502 \pm 0.031)\,\mathrm{ps}^{-1}$

Table 5. Experimental values [38] and SM predictions [57] for meson mixing observables.

3.2 Kaon physics

Analogously to B physics, several operators in table 1 induce $s \to d$ transitions, driving FCNC decays of kaons. The list of observables we considered in this work and the corresponding experimental measurements are reported in table 4, while more details can be found in appendix A. The discussion for kaon physics follows the same lines as the one above for B decays: the relevant coefficients constrained by each observables are reported in table 3. Bounds on WC from rare kaon decays involving leptons are less relevant then the corresponding ones of B mesons, mainly due to the strong constraints from $R_{K^{(*)}}$ and $B_s \to \mu\mu$, while $K \to \pi\nu\bar{\nu}$ gives competitive bounds on $C_{lq}^{(1/3),33}$, see the relevant discussions in section 4.

3.3 $\Delta F = 2$

Meson mixing observables offer some of the most stringent constraints for several scenarios of beyond the SM physics. Among the top quark operators we consider, $\mathcal{O}_{qq}^{(1,3)}$ induce tree-level contributions to these processes, while many more contribute at the loop level.

Model-independent expressions of new physics contributions to $\Delta F = 2$ amplitudes in terms of SMEFT coefficients have been derived in ref. [58]. The authors considered hadronic matrix elements of the various LEFT operators at the low scale, the RG evolution to the electroweak scale, the matching to SMEFT coefficients in the Warsaw basis (and the up quark mass basis), and finally the SMEFT RG evolution up to a scale $\Lambda = 5\,\mathrm{TeV}$. We

neglect the small mismatch in the RG evolution between this scale and the scale at which we define our coefficients, 1 TeV, as this can be well included among the theory uncertainties of working with the LL RG evolution. For the predictions of the SM contribution to meson mixing we use the results of ref. [57], specifically the values obtained with the exclusive V_{cb} measurements and the inclusive V_{ub} one (so-called hybrid scenario). Finally, we take the experimental values for ϵ_K, ΔM_s, and ΔM_d from the PDG combination [38]. In table 5 we collect the values employed in our analysis, where experimental and theory uncertainties are added in quadrature.

3.4 Cabibbo angle decays

Nuclear beta, baryon, pion, kaon decay and semileptonic tau decay data are also precise new physics probes. Since the studied decay modes in the SM are suppressed by $\mathcal{O}\left(\frac{1}{v^2}\right)$, new physics contributions to the observables are only suppressed with respect to the SM by $\mathcal{O}\left(\frac{v^2}{\Lambda^2}\right)$. Taking into account the per-mil level precision reached in some of the observables, potential new physics beyond the TeV scale is probed by these decays. Within the SM picture, this sector is known to lead to some tensions, known as Cabibbo anomalies. It is then interesting to incorporate it to the analysis and to check whether, within our BSM set-up, constraints from other observables leave room for potential new physics explanations of these anomalies.

We make use the global analysis to those observables made in ref. [59] in terms of low-energy EFT coefficients ϵ_i, which updates the EFT analyses made in refs. [60, 61] and incorporates hadronic tau decays. Consistently with the assumptions of that analysis, we match the ϵ_i to the LEFT and then to the SMEFT at tree-level (see A.8). The leading contributions induced by the studied top operators appear through leading logs in the SMEFT running proportionally to the top Yukawa squared.

In our BSM set-up, the combined fit to this set of observables translates into $\mathcal{O}(\text{TeV})$ sensitivity to $C_{lq}^{(3),\ell\ell}$. At least part of the Cabibbo tension can in principle be alleviated by a nonzero $C_{lq}^{(3),22}$ value, which can play an important role in the unitarity relation. In section 5.2 we discuss a UV model inspired by this anomaly. Currently, efforts in the area are focused in understanding whether the so-called Cabibbo anomalies are genuine new physics hints or due to underestimated uncertainties. Overall one may not expect any major improvement in the sensitivity to new physics with respect to the quoted precision from this sector in the short term.

3.5 Magnetic moments and LFU in τ decays

The anomalous magnetic moments of electrons and muons, $a_\ell = (g_\ell - 2)/2$, are among the most precisely measured quantities in experimental physics,

$$
\begin{aligned}
a_e^{\text{exp}} &= (11596521807.3 \pm 2.8) \times 10^{-13}, \\
a_\mu^{\text{exp}} &= (11659205.9 \pm 2.2) \times 10^{-10}.
\end{aligned}
\tag{3.5}
$$

Remarkably, the theoretical precision of the corresponding SM predictions is similar, making them stringent SM tests. In practice, some tensions in the associated evaluations using

Observable	Experimental value	
	$\ell = e$	$\ell = \mu$
Δa_ℓ	$(2.8 \pm 7.4) \times 10^{-13}$	$(20.0 \pm 8.4) \times 10^{-10}$
$g_\tau / g_\ell - 1$	$(2.7 \pm 1.4) \times 10^{-3}$	$(0.9 \pm 1.4) \times 10^{-3}$

Table 6. BSM contributions to anomalous magnetic moment of the leptons, $\Delta a_\ell \equiv a_\ell^{\mathrm{exp}} - a_\ell^{\mathrm{SM}}$, and LFU in τ decays [62], $g_\tau / g_\ell - 1$. The correlation between the g_τ / g_e and the g_τ / g_μ values is of a 51 %.

different inputs slightly limit the current precision. Namely, as pointed out in ref. [63], the value of a_e^{SM} is sensitive to the input value of the fine-structure constant, α_{QED}, and the two most precise determinations, based on Cesium and Rubidium atomic recoils [64, 65], differ by more than 5σ. Similarly, the SM leading-order hadronic vacuum polarization (HVP) prediction quoted in the muon $g - 2$ Theory White Paper (WP) [66–86], which constitutes the dominant source of uncertainty for a_μ^{SM}, is 2σ below the lattice BMW value [87] and new results on related observables [87–100] suggest that the source of the difference may go beyond a mere statistical fluctuation. We then take the weighted average of the a_e^{SM} result obtained from $\alpha_{\mathrm{QED}}^{\mathrm{Cs}}$ and $\alpha_{\mathrm{QED}}^{\mathrm{Rb}}$ and the weighted average of the a_μ^{SM} one using $a_{\mu,\mathrm{BMW}}^{\mathrm{HVP,LO}}$ and $a_{\mu,\mathrm{WP}}^{\mathrm{HVP,LO}}$ as inputs, but adding half their differences as additional sources of systematic uncertainties. The corresponding values of $\Delta a_\ell = a_\ell^{\mathrm{exp}} - a_e^{\mathrm{SM}}$ are compiled in table 6.

The main way to generate an extra a_ℓ contribution in our BSM set-up is through the $\mathcal{O}_{lequ}^{(3),\ell\ell}$ operator, since top-antitop annihilation will generate, through mixing, the dipole operator associated to the anomalous magnetic moment. The process has been recently studied within the LEFT-SMEFT framework in ref. [63]. Using the results from that reference, running up to $\Lambda = 1\,\mathrm{TeV}$ and keeping only the studied operators we find, in TeV units,

$$
\begin{aligned}
\Delta a_e &= -4.8 \times 10^{-8}\, C_{lequ}^{(3),11} + 7.1 \times 10^{-11}\, C_{lequ}^{(1),11}, \\
\Delta a_\mu &= -1.0 \times 10^{-5}\, C_{lequ}^{(3),22} + 1.5 \times 10^{-8}\, C_{lequ}^{(1),22}.
\end{aligned}
\tag{3.6}
$$

Thus, barring some bizarre cancellation mechanism, $|C_{lequ}^{(3),11}| \gtrsim 10^{-4}\,\mathrm{TeV}^{-2}$ and $|C_{lequ}^{(3),22}| \gtrsim 10^{-3}\,\mathrm{TeV}^{-2}$ at $\Lambda = 1\,\mathrm{TeV}$ can already be excluded by current g-2 measurements.

Ratios of leptonic decays of τ and μ provide very clean tests of lepton flavor universality [62, 101]. Deviation from the SM predictions are often parameterized by ratios of effective charges, $g_\ell / g_{\ell'}$, which in the SM limit are equal to 1, and whose experimental values are given in table 6. In the LEFT one has

$$
\begin{aligned}
\frac{g_\tau}{g_e} - 1 &= \frac{v^2}{2} \left(L^{V,LL}_{\substack{\nu e \\ \mu e e \mu}} - L^{V,LL}_{\substack{\nu e \\ \tau \mu \mu \tau}} \right), \\
\frac{g_\tau}{g_\mu} - 1 &= \frac{v^2}{2} \left(L^{V,LL}_{\substack{\nu e \\ \mu e e \mu}} - L^{V,LL}_{\substack{\nu e \\ \tau e e \tau}} \right),
\end{aligned}
\tag{3.7}
$$

Observable	Experimental limit		Observable	Experimental limit
$\mathcal{B}(\mu \to e\gamma)$	5.0×10^{-13} [102]		$\mathcal{B}(\tau \to e\pi^+\pi^-)$	2.7×10^{-8} [108]
$\mathcal{B}(\mu \to 3e)$	1.2×10^{-12} [103]		$\mathcal{B}(\tau \to eK^+K^-)$	4.1×10^{-8} [108]
$\mathcal{B}(\mu\,\mathrm{Au} \to e\,\mathrm{Au})$	8.3×10^{-13} [104]		$\mathcal{B}(\tau \to \mu\gamma)$	5.0×10^{-8} [109]
$\mathcal{B}(\tau \to e\gamma)$	3.9×10^{-8} [105]		$\mathcal{B}(\tau \to 3\mu)$	2.5×10^{-8} [106]
$\mathcal{B}(\tau \to 3e)$	3.2×10^{-8} [106]		$\mathcal{B}(\tau \to \mu\,\bar{e}e)$	2.1×10^{-8} [106]
$\mathcal{B}(\tau \to e\,\bar{\mu}\mu)$	3.2×10^{-8} [106]		$\mathcal{B}(\tau \to \mu\pi^0)$	1.3×10^{-7} [110]
$\mathcal{B}(\tau \to e\pi^0)$	9.5×10^{-8} [107]		$\mathcal{B}(\tau \to \mu\eta)$	7.7×10^{-8} [107]
$\mathcal{B}(\tau \to e\eta)$	1.1×10^{-7} [107]		$\mathcal{B}(\tau \to \mu\eta')$	1.5×10^{-7} [107]
$\mathcal{B}(\tau \to e\eta')$	1.9×10^{-7} [107]		$\mathcal{B}(\tau \to \mu\pi^+\pi^-)$	2.5×10^{-8} [108]
			$\mathcal{B}(\tau \to \mu K^+K^-)$	5.2×10^{-8} [108]

Table 7. Current 95% CL limits on studied LFV branching ratios.

where $v \approx 246\,\mathrm{GeV}$. In our set-up this translates, for $\Lambda = 1\,\mathrm{TeV}$, into

$$\frac{g_\tau}{g_e} - 1 = 0.0038\,(C_{lq}^{(3),33} - C_{lq}^{(3),11})\,,$$
$$\frac{g_\tau}{g_\mu} - 1 = 0.0038\,(C_{lq}^{(3),33} - C_{lq}^{(3),22})\,,$$

(3.8)

where the C_{lq} coefficients are in TeV^{-2} units.

3.6 Charged Lepton Flavor-Violating decay modes

Experimental searches of neutrinoless lepton flavor-violating decay modes of leptons are suitable to test potential BSM scenarios at energy scales beyond the reach of searches at high-energy colliders.

The very stringent limits on $\mu \to e\gamma$, $\mu \to 3e$ transitions and $\mu \to e$ conversion in nuclei, currently coming respectively from MEG at PSI and SINDRUM [102–104], constitute a BSM probe of scales of up to $\Lambda_{\mathrm{BSM}} \sim 10^3 - 10^4\,\mathrm{TeV}$ [111]. They were studied within the LEFT in ref. [112]. For our specific SMEFT set-up, the corresponding limits translate into limits on linear combinations of Wilson coefficients involving semileptonic operators that violate lepton flavour. They are the only operators that at the same time contain the needed BSM LFV insertion and satisfy the assumed top-philic condition. If only one (but any) parameter is switched on, one is able to constrain it at the $|C_i| \lesssim 10^{-4}\,\mathrm{TeV}^{-2}$ level. Studies at PSI, MEG II [113], Mu2e [114] and Mu3e [115], are expected to significantly improve these limits in the near future. We compile the present bounds in table 7.

While the EFT description at the SMEFT-LEFT level of the tau decays is qualitatively equivalent, leading to bounds on Wilson coefficients to the same kind of semileptonic operators for our case, the underlying LFV studies are different [116–119]. With the existing and future probes one does not expect to test new physics much higher than $\Lambda_{\mathrm{BSM}} \sim 10\,\mathrm{TeV}$ [111]. However, many more potential decay channels can be experimentally accessed, as a consequence of a tau mass that is large enough to produce hadrons.
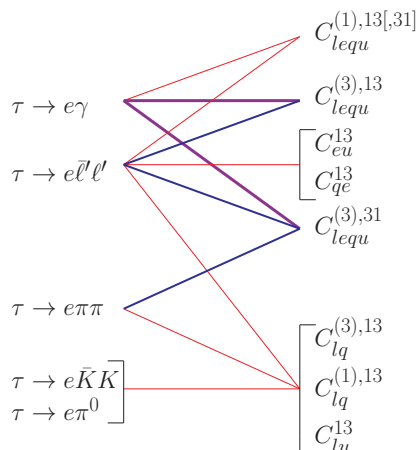
Figure 2. Sensitivity of the different $\tau \to e$ decay modes (similar hierarchy is observed for the $\tau \to \mu$ ones) to the different studied Wilson coefficients using the current experimental bounds. Red, blue and purple lines correspond, respectively, to upper bounds to the coefficient below 0.4, 4×10^{-3} and 4×10^{-4} (TeV units), assuming one parameter is present at a time.

In this sense, if charged LFV were discovered in the tau sector, the information from the different decay channels would unlock the full power of the EFT approach to stringently discriminate among different BSM scenarios, by having direct experimental access to the values of the different Wilson Coefficients. In the meantime we can use the existing limits to set bounds on different combinations of them. Current limits, coming from Belle and BaBar [38], are expected to be improved by Belle-II [120]. In figure 2 the sensitivity of the different decay modes to the different studied operators is shown.

3.7 Electroweak and Higgs data

Electroweak precision data (Z and W decays) and Higgs measurements provide strong indirect constraints on new physics involving the top quark, via loop effects. The authors of ref. [121] performed a global SMEFT analysis of Z and W pole data, WW pair production data at LEP2, and Higgs signal strength measurements from ATLAS and CMS. SMEFT contribution in the Warsaw basis are included at the tree-level except for observables that are loop-generated in the SM (such as $h \to \gamma\gamma$, $Z\gamma$ and $gg \to h$), in which case one-loop contributions are included as well. For our numerical analysis we use updated results for the global fit (including correlations), kindly provided by the authors of ref. [121]. The constraints on LFV Z couplings to charged leptons are taken from the fit in ref. [122], while those the LFV couplings to neutrinos are constrained via the measurement of the effective number of neutrinos N_ν updated in ref. [123]. The fit is performed in terms of specific combinations of Wilson coefficients of the Warsaw basis evaluated at the weak scale shown in table 8. Their definition is reported in appendix A.9.

We interpret the resulting likelihood for SMEFT coefficients as evaluated at the EW scale (we fix it at M_Z for concreteness), and then include the RG evolution up to 1 TeV to obtain the final likelihood for our analysis, in terms of the coefficients of the operators

C_W	δc_z	$c_{z\square}$	c_{gg}	$c_{\gamma\gamma}$	c_{zz}	$c_{z\gamma}$
$[\delta g_L^{W\ell}]_{\alpha\beta}$	$[\delta g_L^{Z\ell}]_{\alpha\beta}$	$[\delta g_R^{Z\ell}]_{\alpha\beta}$	$[\delta g_L^{Zd}]_{\alpha\alpha}$	$[\delta g_R^{Zd}]_{\alpha\alpha}$	$[\delta g_L^{Zu}]_{\alpha\alpha}$	$[\delta g_L^{Zu}]_{\alpha\alpha}$
$[C_{uH}]_{33}$	$[C_{dH}]_{33}$	$[C_{eH}]_{22}$	$[C_{eH}]_{33}$	$[C_{ll}]_{1221}$		

Table 8. List of Wilson coefficients used in the fit of ref. [121]. The ones with capital C are already in the Warsaw basis, while the definition of the others is reported in appendix A.9.

listed in table 1. The coefficients that provide relevant constraints to our analysis are listed here, together with the TeV-scale coefficients that contribute the most to each one:

$$
\begin{aligned}
\text{EW/Higgs coeff.} && \text{TeV-scale coefficient} \\
\delta g_L^{Z\ell} &\longleftarrow & C_{uB},\ C_{uW}, C_{Hu},\ C_{Hq}^{(1,3)},\ C_{lq}^{(1,3),\ell\ell},\ C_{lu}^{\ell\ell},\ \ldots \\
\delta g_L^{W\ell} &\longleftarrow & C_{uB},\ C_{uW},\ C_{Hu},\ C_{Hq}^{(1,3)},\ C_{lq}^{(3),\ell\ell},\ \ldots \\
\delta g_R^{Z\ell} &\longleftarrow & C_{uB},\ C_{uW},\ C_{Hu},\ C_{Hq}^{(1,3)},\ C_{eu}^{\ell\ell},\ C_{qe}^{\ell\ell},\ \ldots \\
\delta g_L^{Zb} &\longleftarrow & C_{Hq}^{(1,3)},\ C_{Hu},\ C_{qq}^{(1,3)},\ \ldots \\
\delta g_R^{Zb} &\longleftarrow & C_{Hq}^{(1)},\ C_{Hu},\ C_{qq}^{(1,3)},\ C_{uB},\ C_{uW},\ \ldots \\
c_{\gamma\gamma} &\longleftarrow & C_{uB},\ C_{uW},\ C_{uG} \\
c_{gg} &\longleftarrow & C_{uG} \\
[C_{eH}]_{\alpha\alpha} &\longleftarrow & C_{lequ}^{(1),\alpha\alpha} \\
[C_{uH}]_{33} &\longleftarrow & C_{uH},\ C_{uG},\ C_{Hq}^{(1,3)},\ C_{qu}^{(1,8)},\ \ldots
\end{aligned}
\tag{3.9}
$$

3.8 Direct bounds from LHC

SMEFT interpretations of top quark production and decay measurements at LHC have been discussed in several works [12, 14, 124–137], providing direct bounds on 4-quark, dipole and Higgs-top operators.

The analysis by the SMEFiT collaboration [130] includes observables from the LHC Run-II dataset and studies connections with Higgs and diboson data. The SMEFiT fitting framework has been released as a Python open source package [135]. We exploit the flexibility of this toolbox to perform a SMEFT analysis of Higgs, top quark and electroweak production data (see section 3 of ref. [130] for details) including our operators of table 1, with exception of the semi-leptonic ones. The resulting constraints are reported in appendix A.10. In the next section we compare these with the indirect constraints derived from our global analysis.

4 Global analysis

The observables described in the previous section, except for the direct constraints from LHC of section 3.8, are used to build the log-likelihood as in eq. (2.2). This provides global indirect constraints on top quark operators, that we can compare with the direct ones from measurements at LHC. In the following we present examples of fits derived using our global likelihood. For simplicity we assume all Wilson coefficients to be real in the following.

Wilson	Global fit [TeV^{-2}]	Dominant
$C_{qq}^{(+)}$	$(-1.9 \pm 2.3) \times 10^{-3}$	ΔM_s
$C_{qq}^{(-)}$	$(-2.0 \pm 1.0) \times 10^{-1}$	$B_s \to \mu\mu$
$C_{qu}^{(1)}$	$(1.3 \pm 1.0) \times 10^{-1}$	ΔM_s
$C_{qu}^{(8)}$	$(-1.7 \pm 4.4) \times 10^{-1}$	ΔM_s
C_{uu}	$(-3.0 \pm 1.7) \times 10^{-1}$	$\delta g_{L,11}^{Ze}$
$C_{Hq}^{(+)}$	$(18.2 \pm 8.9) \times 10^{-3}$	$B_s \to \mu\mu$
$C_{Hq}^{(-)}$	$(5.9 \pm 4.5) \times 10^{-2}$	$\delta g_{L,11}^{Ze}$
C_{Hu}	$(-4.3 \pm 2.3) \times 10^{-2}$	$\delta g_{L,11}^{Ze}$
C_{uB}	$(-0.6 \pm 2.0) \times 10^{-2}$	$c_{\gamma\gamma}$
C_{uG}	$(-0.1 \pm 2.0) \times 10^{-2}$	c_{gg}
C_{uH}	$(-0.3 \pm 5.2) \times 10^{-1}$	$C_{uH,33}$
C_{uW}	$(0.0 \pm 3.1) \times 10^{-2}$	$c_{\gamma\gamma}$

Table 9. Combined fit for one at a time Wilson coefficients for nonleptonic operators. The dominant observable giving the most precise bound is also displayed.

4.1 One-parameter fits

First, we perform one-parameter fits setting all the Wilson coefficients to zero except for one. While such one-parameter set-up is not a realistic low-energy description of typical UV scenarios, it can provide meaningful information about the new physics scale that can be probed if that operator is generated. It also provides a way to compare the sensitivity of different observables or, alternatively, which observables/sectors one should look at first if a specific operator is induced by the studied UV model.

The results associated to the different operators, respectively nonleptonic, semileptonic lepton-flavor conserving and semileptonic lepton-flavor violating, are shown in tables 9, 10 and 11, together with which (isolated) single observable currently gives the most precise determination of the associated Wilson coefficient. We have defined $C_{iq}^{(\pm)} \equiv C_{iq}^{(1)} \pm C_{iq}^{(3)}$ for $i = H, q, l$. As shown in section 3, these linear combinations are typically the ones appearing at leading order in the most constraining observables.

We study next the complementarity of the indirect bounds with the direct LHC ones. In figure 3 we show the results of the individual fits for Higgs-Top, Dipoles and Four Quarks operators, together with corresponding bounds derived through the SMEFiT fitting framework. We stress that, exclusively in this plot, Wilson coefficients are displayed according to the SMEFiT basis (lower case c_{AB}), whose expression in terms of the Warsaw basis can be found in table 14.

A few comments are in order concerning the comparison of these bounds. The combinations involving the coefficients $C_{qq}^{(1/3)}$ are constrained up to the 10^{-2} level, due to the

Wilson	Global fit [TeV^{-2}]	Dominant	Wilson	Global fit [TeV^{-2}]	Dominant
$C_{lq}^{(+),11}$	$(2.4 \pm 3.5) \times 10^{-3}$	R_K	C_{eu}^{11}	$(5.0 \pm 8.1) \times 10^{-2}$	$\Delta g_R^{Ze}{}_{11}$
$C_{lq}^{(+),22}$	$(-4.0 \pm 3.4) \times 10^{-3}$	R_K	C_{eu}^{22}	$(4.6 \pm 2.2) \times 10^{-1}$	$\Delta g_R^{Ze}{}_{22}$
$C_{lq}^{(+),33}$	$(7.2 \pm 4.4) \times 10^{-1}$	g_τ/g_i	C_{eu}^{33}	$(-2.3 \pm 2.5) \times 10^{-1}$	$\Delta g_R^{Ze}{}_{33}$
$C_{lq}^{(-),11}$	$(10.1 \pm 7.7) \times 10^{-2}$	$R_{K^{(*)}}^\nu$	$C_{lequ}^{(1),11}$	$(0.4 \pm 1.0) \times 10^{-2}$	$(g-2)_e$
$C_{lq}^{(-),22}$	$(-7.4 \pm 7.0) \times 10^{-2}$	$R_{K^{(*)}}^\nu$	$C_{lequ}^{(1),22}$	$(1.8 \pm 1.6) \times 10^{-2}$	C_{eH22}
$C_{lq}^{(-),33}$	$(-22.1 \pm 9.6) \times 10^{-2}$	$R_{K^{(*)}}^\nu$	$C_{lequ}^{(1),33}$	$(8.0 \pm 9.1) \times 10^{-2}$	C_{eH33}
C_{lu}^{11}	$(-1.7 \pm 7.0) \times 10^{-2}$	$\delta g_{L,11}^{Ze}$	$C_{lequ}^{(3),11}$	$(-0.6 \pm 1.5) \times 10^{-5}$	$(g-2)_e$
C_{lu}^{22}	$(-4.3 \pm 1.8) \times 10^{-1}$	$\delta g_{L,22}^{Ze}, R_K$	$C_{lequ}^{(3),22}$	$(-19.3 \pm 8.1) \times 10^{-5}$	$(g-2)_\mu$
C_{lu}^{33}	$(0.5 \pm 2.4) \times 10^{-1}$	$\Delta g_{L,33}^{Ze}$	$C_{lequ}^{(3),33}$	$(-7.0 \pm 7.8) \times 10^{-1}$	C_{eH33}
C_{qe}^{11}	$(-0.7 \pm 3.9) \times 10^{-2}$	R_{K^*}			
C_{qe}^{22}	$(12.1 \pm 9.2) \times 10^{-3}$	$B_s \to \mu\mu$			
C_{qe}^{33}	$(2.2 \pm 2.4) \times 10^{-1}$	$\delta g_{R,33}^{Ze}$			

Table 10. Combined fit for one at a time Wilson coefficients for semileptonic lepton-flavor-conserving operators. For reference, we also display the single observable giving the most precise bound.

Wilson	$\mu \to e$		$\tau \to \mu$		$\tau \to e$	
	Limit	Dominant	Limit	Dominant	Limit	Dominant
$C_{lequ}^{(3)}$	3.9×10^{-9}	$\mu \to e\gamma$	5.0×10^{-5}	$\tau \to \mu\gamma$	4.4×10^{-5}	$\tau \to e\gamma$
$C_{lequ}^{(1)}$	3.6×10^{-5}	$\mu \to 3e, e\gamma$	2.7×10^{-2}	$\tau \to \mu\gamma$	2.4×10^{-2}	$\tau \to e\gamma$
$C_{lq}^{(3)}$	6.7×10^{-5}	$\mu\mathrm{Au} \to e\mathrm{Au}$	6.8×10^{-2}	$\tau \to \mu\pi\pi$	7.0×10^{-2}	$\tau \to e\pi\pi$
$C_{lq}^{(1)}$	4.0×10^{-5}	$\mu\mathrm{Au} \to e\mathrm{Au}$	9.8×10^{-2}	$\tau \to \mu\pi\pi$	1.0×10^{-1}	$\tau \to e\pi\pi$
C_{lu}	4.0×10^{-5}	$\mu\mathrm{Au} \to e\mathrm{Au}$	1.0×10^{-1}	$\tau \to \mu\pi\pi$	1.1×10^{-1}	$\tau \to e\pi\pi$
C_{eu}	3.6×10^{-5}	$\mu\mathrm{Au} \to e\mathrm{Au}$	1.9×10^{-1}	$\tau \to \mu ee$	2.1×10^{-1}	$\tau \to 3e$
C_{qe}	3.6×10^{-5}	$\mu\mathrm{Au} \to e\mathrm{Au}$	2.2×10^{-1}	$\tau \to \mu ee$	2.1×10^{-1}	$\tau \to 3e$

Table 11. Upper limits (68 % CL) in TeV^{-2} for the different LFV Wilson coefficients. Family superscripts are omitted (in the working approximation bounds on $C_{lequ}^{(1,3),ij}$ and $C_{lequ}^{(1,3),ji}$ are found to be the same). For reference we also display the single observable giving the most precise bound.
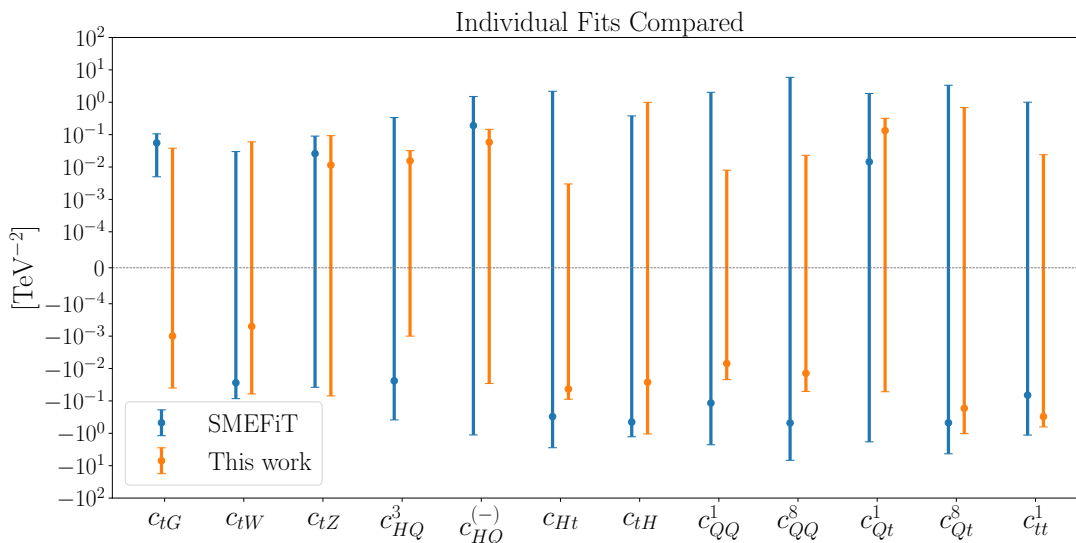
Figure 3. Comparison of the indirect constraints derived in this work and the direct bounds obtained through the SMEFiT toolbox. We display the 95% CL bounds for Wilson coefficients in the SMEFiT basis and notation (see table 14 for their expression in terms of the Warsaw basis).

$\Delta F = 2$ meson mixing observables that strongly constrain their sum. This result remarkably improves the bounds derived by the ATLAS and CMS direct measurements of top quark cross-sections by 2-3 orders of magnitude. An improvement is also clear for the combinations of the Higgs-Top operators $C_{Hq}^{(1/3)}$ and C_{Hu} (c_{Ht}), mostly constrained in this analysis by the electroweak and Higgs observables discussed in section 3.7. The C_{uG} (c_{tG}) coefficient represents the only exception to the general improvement trend observed in almost all the cases. However, as discussed in ref. [130], the numerical fit of C_{uG} performed through the SMEFiT routine seems to be unstable, so that we do not consider this direct bound reliable (see section 5.3 of ref. [130] for an extended discussion).

4.2 Two-parameters fits

In this section we carry out two-parameter fits, i.e. two Wilson coefficients at a time are allowed to vary under the assumption that they are generated at the same scale, while all the others are set to zero. These analyses can provide useful information on the interplay between pairs of coefficients, highlighting what are the most constrained combinations and giving thus intuition on their correlations. This is also the first step towards a UV interpretation, as WC's allowed regions can be contrasted with the relations predicted by specific UV scenarios. Among all the possible pairs we only show some interesting cases, e.g. when the importance of combining different sectors is highlighted and/or when the pair can be interesting from a NP perspective.

The results of two-parameters fits are illustrated in figures 4–9. We display the 68%CL regions obtained when different subsets of data are taken as input and the 68% and 95%CL regions resulting from the whole set of observables. In order to better understand the underlying phenomenology, in some plots we also show single-observable 1σ contours. In
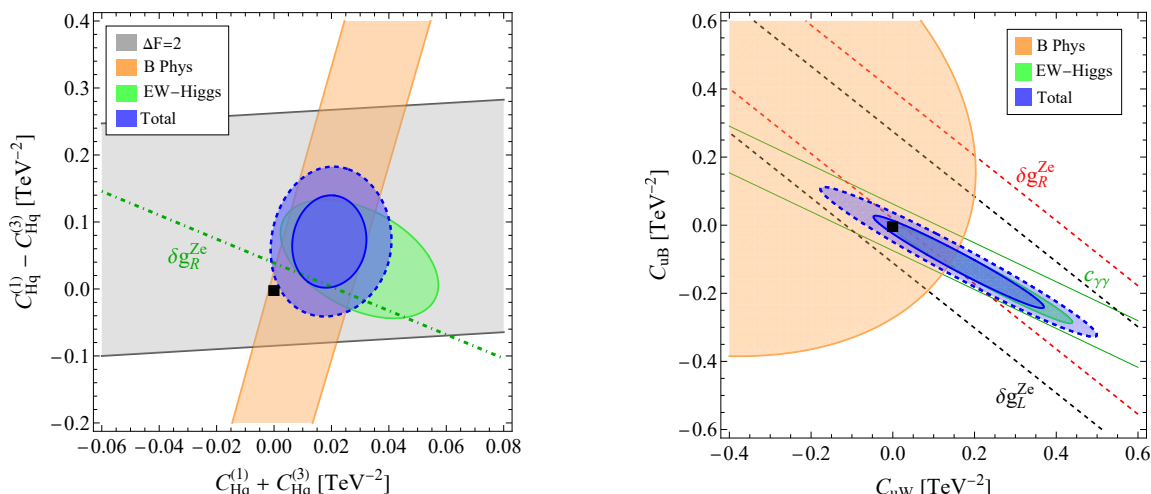
Figure 4. Left panel: Higgs-Top coefficients $C_{Hq}^{(+)}$ vs $C_{Hq}^{(-)}$. Right panel: dipole coefficients C_{uW} vs C_{uB}.
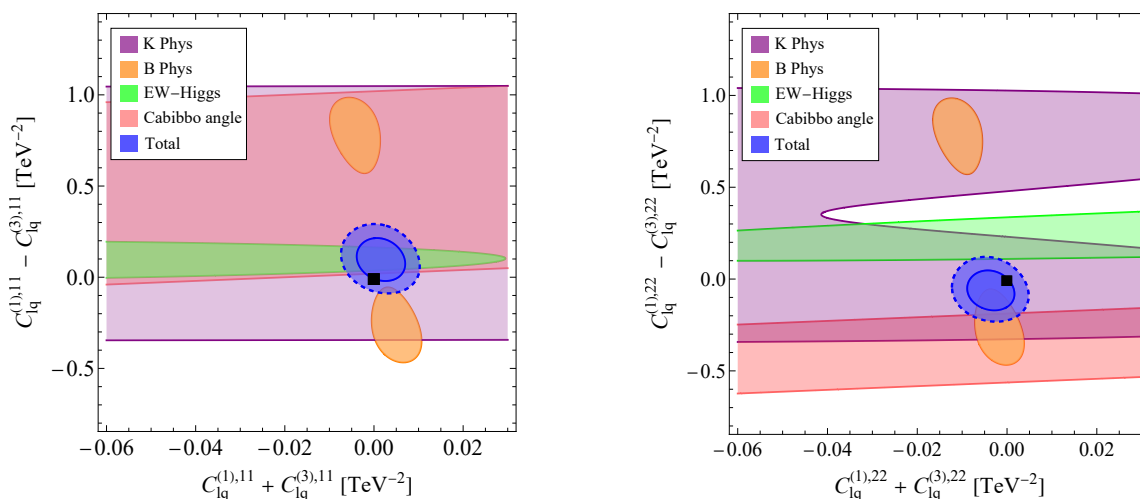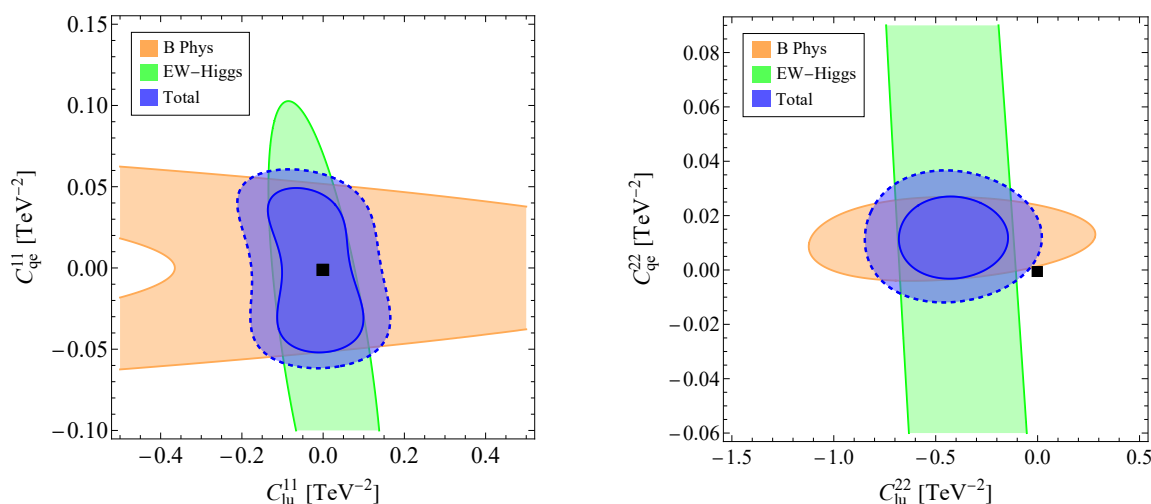

Figure 5. Semileptonic $C_{lq}^{(+)}$ vs $C_{lq}^{(-)}$ coefficients involving electrons and muons.

this way, we can investigate the constraining power of each sector/observable on coefficients pairs.

To start with, in figure 4 we show the allowed regions for the $C_{Hq}^{(+)}$ and $C_{Hq}^{(-)}$ coefficients. Noteworthy, constraints from the B sector, mostly due to leptonic $B \to \ell\ell$ and radiative decays, are competitive to the EW and Higgs bounds, resulting in a (slightly more than) 2σ deviation from the SM prediction. This pull is mostly due to the Z boson coupling to right-handed electrons, $\delta g_R^{Ze} = (-7.3 \pm 4.4) \times 10^{-3}$ [121], as we show in the plot with the dot-dashed green line marking the 1σ bound. In the right panel, as an example of dipole operators, we show the C_{uW} vs C_{uB} plane. As expected, a strong constraint is set on the photon direction, whose main responsible is the $c_{\gamma\gamma}$ coefficient discussed in section 3.7. The dominant constraints on the orthogonal direction are set again by the electroweak
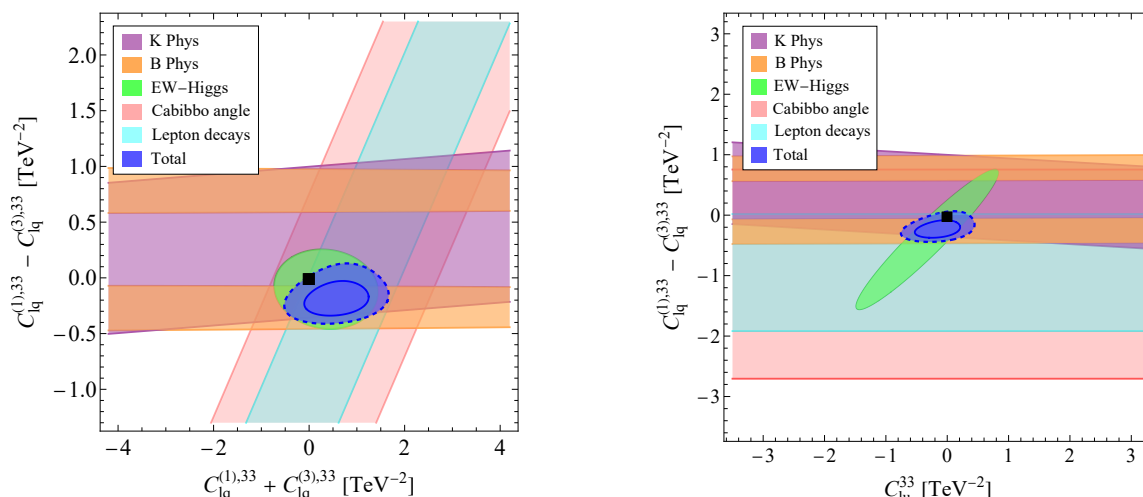
Figure 6. Left panel: semileptonic $C_{lq}^{(+)}$ vs $C_{lq}^{(-)}$ coefficients involving tau leptons. Bounds from the EW sector are improved by the synergy with the other sectors. Right panel: semileptonic $C_{lq,33}^{(-)}$ vs $C_{lu,33}$ coefficients.

Figure 7. Here we show the semileptonic coefficients C_{lu} vs. C_{qe} for electrons (left) and muons (right).

sector, as a combined effect of the deviations in the Z boson coupling to leptons and other (pseudo-)observables.

In figure 5 and the left panel of figure 6, we show the two-parameters fits for the $C_{lq}^{(+/-),\alpha\alpha}$ coefficients. The existence of flat directions points out the importance of performing SMEFT analysis using various datasets, exploiting the complementarity between different physics sectors to constraint the EFT space. Focussing on B-physics, the strong bound on the positive combinations $C_{lq}^{(+),\alpha\alpha}$, with $\alpha = 1, 2$, can be ascribed to the $R_{K^{(*)}}$ measurements. In addition, the recently announced measurement of R_K^ν, with a pull from the SM, drives the allowed region for the negative combination, splitting the allowed band
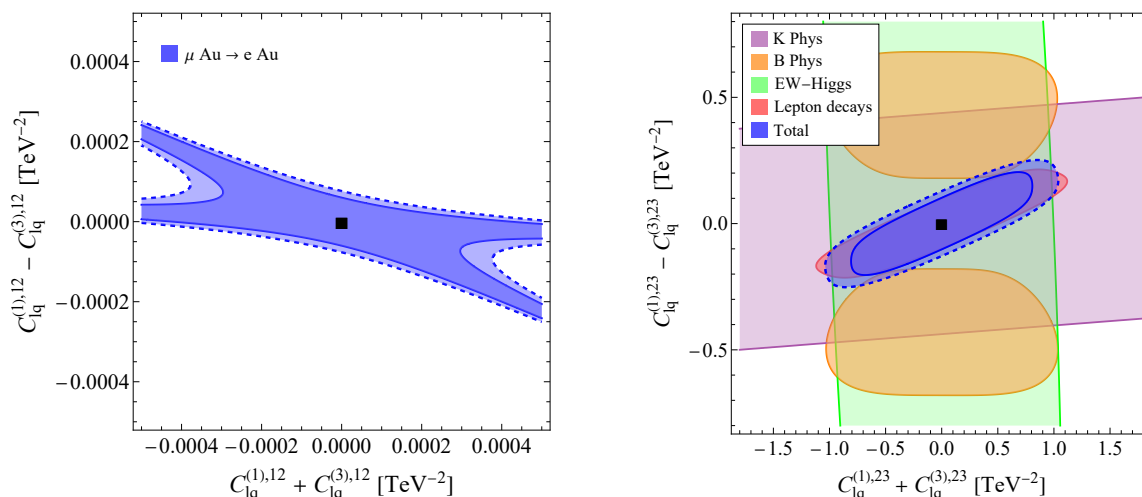
Figure 8. Two-parameters fit for the LFV semileptonic coefficients $C_{lq,12}^{(+/-)}$ and $C_{lq,23}^{(+/-)}$. The stronger constraints come from the LFV decay modes of tau lepton.

in two regions depending on the interference with the SM. Interestingly, in case of electrons and muons (figure 5) the deviation in R_K^ν could be compatible with the Cabibbo angle anomaly but is in some tension with the bounds from EW precision data, which drives the global fit towards the SM. In case of tau leptons (figure 6), instead, the looser EW bounds and the vanishing contribution to R_K allow the global analysis to overlap with the preferred region from R_K^ν. This feature is visible also in the right panel of figure 6, where we display the allowed regions in the plane $C_{lq}^{(-),33}$ vs C_{lu}^{33}. The semileptonic coefficients $C_{lq}^{(1,3),33}$ will be further discussed in section 5, where the scenario of a single scalar leptoquark S_1 coupling tau leptons and top quarks is explored. In figure 7 we show the fit in the plane of C_{lu} vs. C_{qe} for both electrons (left panel) and muons (right panel). In both cases the global fit shows an interesting interplay of B and EW physics.

In figure 8, we show the pairwise fits on the LFV coefficients $C_{lq,12}^{(+/-)}$ and $C_{lq,23}^{(+/-)}$. In the first case, the global fit is controlled entirely by the $\mu\text{Au} \to e\text{Au}$ measurement, as expected from table 11. In the second case, the sensitivity of the coefficients is mostly driven by the tau LFV decays discussed in section 3.6. However, LFV decay modes of B and K mesons, as well bounds on LFV Z decays, can improve the constraints. This discussion also applies to the $C_{lq,13}^{(+/-)}$ coefficients, whose bounds are very similar to the ones derived for $C_{lq,23}^{(+/-)}$.

Regarding four-quark operators, it is clear from the left panel of figure 9 that the combinations $C_{qq}^{(+)}$ and $C_{qq}^{(-)}$ are the relevant degrees of freedom in the EFT space. In particular, the sum is severely constrained by meson oscillations, while the orthogonal combination is mainly constrained by $B_s \to \mu^+\mu^-$, kaon decays and EW and Higgs observables. In the right panel we display the $C_{qu}^{(1)}$ vs $C_{qq}^{(+)}$ pair. We illustrate the effect of the δg_R^{Ze} measurement, responsible again for the main discrepancy in the EW sector. The resulting allowed region shows a tension from the SM value within of slightly more than two sigmas.
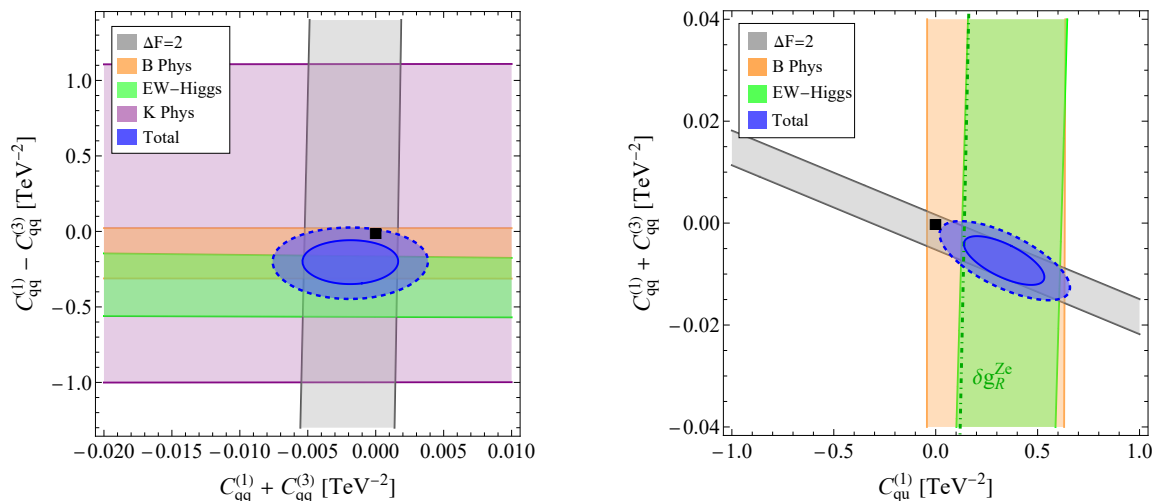
Figure 9. Left panel: four-quarks $C_{qq}^{(1)+(3)}$ vs $C_{qq}^{(1)-(3)}$ coefficients. $\Delta F = 2$ processes constraint the $C_{qq}^{(+)}$ combination up to the 10^{-3} level. The difference is constrained by the other sectors. Right panel: $C_{qu}^{(1)}$ and $C_{qq}^{(+)}$.

4.3 Gaussian fit with no semileptonic operators

Plots pose a limitation in only allowing fits to pairs of coefficients. There are two main possibilities to go beyond that: providing the complete likelihood or employing the Gaussian approximation around the global maximum of the likelihood to derive a multi-dimensional fit. While the former solution is more general, it is not a fit and the complexity of our analysis make the resulting numerical function unwieldy to publish in a paper.[3] Therefore, in this work we opt to perform a multi-dimensional Gaussian fit.

We consider all the operators in table 1 except the semileptonic ones:[4]

$$\vec{C} = (C_{qq}^{(+)}, C_{qq}^{(-)}, C_{uu}, C_{qu}^{(1)}, C_{qu}^{(8)}, C_{Hq}^{(+)}, C_{Hq}^{(-)}, C_{Hu}, C_{uH}, C_{uG}, C_{uW}, C_{uB}) \, . \tag{4.1}$$

The best-fit point improves the χ^2 from the SM value by $\Delta\chi^2 \equiv \chi^2_{\text{SM}} - \chi^2_{\text{best-fit}} \approx 10.9$. This comes mostly from the EW-Higgs sector, however it is a result in mild improvements in several observables rather than a resolution of a specific large anomaly. The fit presents some almost flat directions, which imply correlations among some coefficients very close to ± 1. For this reason, we report the result in terms of the eigenvectors of the Hessian matrix around the best-fit minimum:

$$\chi^2 = \chi^2_{\text{best-fit}} + (C_i - \mu_{C_i})(\sigma^2)^{-1}_{ij}(C_j - \mu_{C_j}) = \chi^2_{\text{best-fit}} + \frac{(K_i - \mu_{K_i})^2}{\sigma^2_{K_i}}. \tag{4.2}$$

The results for the best-fit values μ_{K_i} and uncertainties σ_{K_i} are reported in table 12, while

---

[3]However, we can provide it in electronic form upon request.

[4]An analogous Gaussian fit including also semileptonic operators does not provide a physically meaningful result. This is due to the non-Gaussianities, that become very important in light of the mild deviations from the SM expectation present in some observables. In this case, performing a Gaussian expansion around the global minimum provides a bad approximation to the full likelihood.

Coefficient	Gaussian fit [TeV^{-2}]	Coefficient	Gaussian fit [TeV^{-2}]
K_1	0.0019 ± 0.0023	K_7	0.56 ± 0.79
K_2	0.0169 ± 0.0083	K_8	0.80 ± 0.88
K_3	-0.001 ± 0.015	K_9	-0.8 ± 1.3
K_4	-0.017 ± 0.021	K_{10}	-1.1 ± 1.7
K_5	0.044 ± 0.029	K_{11}	20.5 ± 12
K_6	-0.26 ± 0.38	K_{12}	-14 ± 15

Table 12. Result of our multidimensional gaussian fit of non-leptonic coefficients, in terms of the eigenvectors of the Hessian matrix.

the rotation matrix from these coefficients to our C_i is given by $\vec{K} = U_{KC}\vec{C}$, with

$$
U_{KC} = \begin{pmatrix}
-1. & 0. & 0. & -0.016 & -0.004 & -0.004 & 0.021 & 0. & 0. & 0. & 0. & 0. \\
-0.005 & -0.089 & -0.015 & 0.058 & 0. & 0.984 & -0.005 & -0.117 & 0. & -0.009 & 0.044 & 0.062 \\
0.004 & 0.011 & -0.039 & 0.018 & -0.001 & -0.1 & 0.145 & -0.28 & 0.015 & -0.494 & 0.447 & 0.667 \\
-0.007 & -0.013 & 0.09 & -0.053 & -0.003 & 0.081 & -0.316 & 0.64 & 0.024 & -0.673 & -0.125 & -0.059 \\
0.005 & 0.007 & -0.074 & 0.042 & -0.002 & -0.025 & 0.258 & -0.525 & 0.025 & -0.549 & -0.213 & -0.55 \\
-0.004 & -0.042 & 0.025 & 0.068 & 0.006 & -0.004 & -0.128 & 0.084 & 0.006 & 0.022 & 0.853 & -0.492 \\
-0.006 & -0.138 & 0.078 & 0.197 & 0.959 & -0.017 & 0.091 & 0.047 & -0.065 & -0.007 & -0.017 & 0.008 \\
0.002 & -0.35 & -0.006 & 0.647 & -0.25 & -0.029 & 0.543 & 0.317 & 0.014 & 0. & -0.013 & 0.006 \\
0.005 & 0.008 & 0.029 & -0.139 & 0.077 & 0.017 & 0.147 & 0.061 & 0.973 & 0.037 & 0.017 & -0.003 \\
0.023 & 0.225 & 0.075 & -0.564 & 0.052 & 0.092 & 0.685 & 0.293 & -0.215 & -0.003 & 0.096 & -0.058 \\
0.006 & -0.863 & 0.263 & -0.408 & -0.057 & -0.062 & -0.037 & -0.099 & -0.041 & 0. & -0.01 & 0.005 \\
-0.003 & 0.232 & 0.95 & 0.158 & -0.071 & 0.012 & 0.007 & -0.117 & 0.005 & 0. & -0.012 & 0.007
\end{pmatrix} . \quad (4.3)
$$

The last two coefficients, K_{11} and K_{12}, correspond to two flat directions with only very weak constraints from our observables, given approximately by:

$$
\begin{aligned}
K_{11} &\approx -0.86 C_{qq}^{(-)} + 0.26 C_{uu} - 0.41 C_{qu}^{(1)} - 0.10 C_{Hu} + \dots , \\
K_{12} &\approx +0.23 C_{qq}^{(-)} + 0.95 C_{uu} + 0.16 C_{qu}^{(1)} - 0.12 C_{Hu} + \dots .
\end{aligned} \quad (4.4)
$$

Using the naive power counting of ref. [138], one may estimate the allowed EFT hyper-volume spanned by the studied non-leptonic Wilson coefficients as $V_{\text{EFT}} \sim \frac{\pi^6}{720} \left(\frac{(4\pi)}{\text{TeV}^2} \right)^3 \left(\frac{(4\pi)^2}{\text{TeV}^2} \right)^8 \left(\frac{(4\pi)^3}{\text{TeV}^2} \right)$, assuming $\Lambda = 1\,\text{TeV}$. From table 12, experimental constraints restrict the potential SMEFT hyperspace to a very tiny fraction of its volume, $\sim 10^{-31}$.

5 Applications for UV models

In this section we apply our global analysis to two UV scenarios of New Physics at the TeV scale, coupled mainly to the top quark. The first is a simple minimal extension of the SM by one scalar leptoquark $S_1 \sim (\bar{\mathbf{3}}, \mathbf{1})_{+1/3}$ coupled only to the third generation quark and lepton doublets. The second scenario is an application guided by the Cabibbo anomaly, it includes the scalar leptoquark $S_3 \sim (\bar{\mathbf{3}}, \mathbf{3})_{+1/3}$ as well as the vector leptoquark $U_1 \sim (\mathbf{3}, \mathbf{1})_{+2/3}$.

5.1 Single leptoquark S_1

Let us consider the scalar leptoquark $S_1 \sim (\bar{\mathbf{3}}, \mathbf{1})_{+1/3}$, coupled only to the third generation of quark and lepton $SU(2)_L$ doublets:

$$
\mathcal{L} \supset \lambda_{t\tau} \, \bar{q}_3^c i\sigma_2 l_3 \, S_1 + \text{h.c.} , \quad (5.1)
$$
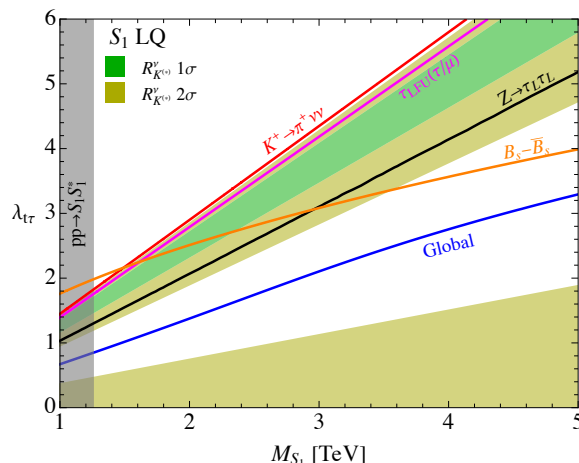
Figure 10. Present constraints on the S_1 leptoquark model, coupled only to third generation quark and lepton doublets. The green (yellow) region is preferred at 1σ (2σ) by $R^\nu_{K^{(*)}}$, while the gray region is excluded at 95%CL from direct searches at LHC. The region above each line is excluded at 95%CL by the corresponding observable, or by our global analysis (blue line).

where $q_3 = (t_L, V_{tj}d^j_L)$, $l_3 = (\nu_\tau, \tau_L)$ and σ_i are the Pauli matrices. While the recent interest in this leptoquark stems from its ability to address the $R(D^{(*)})$ and $(g-2)_\mu$ anomalies, our setup will not address either of those since in our case S_1 doesn't couple to the charm nor the muon. Indeed, our goal is only to showcase a simple application of the global analysis.

Matching at tree level this Lagrangian to the SMEFT gives [139, 140]

$$C^{(1),33}_{lq} = -C^{(3),33}_{lq} = \frac{|\lambda_{t\tau}|^2}{4M_{S_1}^2} \ . \tag{5.2}$$

For precision studies of such scenarios, however, the tree level matching is not sufficient since one-loop contributions can be important for some observables, as discussed in refs. [141–146]. For our goal it is sufficient to add the leading contributions to four-quark operators, which induce contributions to meson-mixing observables. From the complete one-loop matching of this scalar leptoquark to SMEFT, done in ref. [147], we extract the relevant contribution:

$$C^{(1)}_{qq} = C^{(3)}_{qq} = -\frac{|\lambda_{t\tau}|^4}{256\pi^2 M_{S_1}^2} \ . \tag{5.3}$$

These coefficients are generated at the M_{S_1} scale, that we assume to be near 1 TeV, so that we neglect the RG evolution between M_{S_1} and 1 TeV.

The constraints from the global analysis, as well as from the most relevant observables, in the plane of the $\lambda_{t\tau}$ coupling vs. the leptoquark mass, are shown in figure 10. The shaded gray region is excluded by ATLAS from leptoquark pair-production searches [148]. The regions preferred at 1σ and 2σ by the $R^\nu_{K^{(*)}}$ combination, eq. (3.3), are show in green and yellow, respectively. Interestingly, the intermediate white region is disfavored at the 95%CL by $R^\nu_{K^{(*)}}$ due to the negative interference with the SM, which suppresses the branching ratio below the 2σ level. We observe an interesting interplay of constraints from different classes

of observables: electroweak precision data and τ physics, meson mixing, B and kaon rare decays, as well as direct searches from LHC.

5.2 Two leptoquarks for the Cabibbo anomaly?

In this section we illustrate how our combined likelihood may also be used to check whether experimental results in tension with the SM predictions can be partially accommodated in top-philic extensions (and which ones), taking into account the restrictions imposed by experimental results in other sectors. Here we focus on the longstanding tensions within the SM involving the determination of the inputs of the first row of the CKM matrix, known as Cabibbo anomalies.

Regardless of whether nonzero values are allowed or not for the remaining Wilson coefficients, the likelihood of the Cabibbo angle observables displays a 3σ preference for a nonzero value of $C_{lq}^{(3),22}$ at $\Lambda = 1\,\text{TeV}$,

$$[C_{lq}^{(3),22}]^{\text{Cabibbo}} = (0.19 \pm 0.06)\,\text{TeV}^{-2}\,. \tag{5.4}$$

Let us first develop on where this preferred nonzero value comes from. $C_{lq}^{(3),\alpha\alpha}$ induces an unusually large $C_{Hl}^{(3),\alpha\alpha}$ at the EW scale, due to a mixing that involves a double top Yukawa insertion. The leading log approximation, which one may expect to give a first approximation for $\Lambda \gtrsim \text{TeV}$, is displayed in eq. (A.39). After EWSB $C_{Hl}^{(3),\alpha\alpha}$ induces, at tree level, a re-scaling of the corresponding lepton charged current vertices, modifying the ratios of muon, beta and kaon decays. As a consequence, the corresponding apparent unitarity relation is[5]

$$\Delta_{\text{CKM}} \equiv |V_{ud}^{\beta}|^2 + |V_{us}^{K_{\ell 3}}|^2 - 1 \approx -2v^2\,(|V_{ud}|^2 C_{Hl}^{(3),22} - |V_{us}|^2 (C_{Hl}^{(3),\ell\ell} - C_{Hl}^{(3),11} - C_{Hl}^{(3),22}))$$

$$\approx -2v^2\,C_{Hl}^{(3),22} \sim -\left[\frac{N_c}{2\pi^2}\frac{m_t^2}{\Lambda_{\text{UV}}^2}\log\frac{\Lambda_{\text{UV}}}{M_Z}\right]\Lambda_{\text{UV}}^2 C_{lq}^{(3),22}(\Lambda_{\text{UV}}^2)\,. \tag{5.5}$$

Experimentally Δ_{CKM} is known beyond the per-mil level and gives the main pull behind the result of eq. (5.4).

If we set all the parameters to zero except for $C_{lq}^{(3),22}$ for the EW/Higgs likelihood, we also obtain a slight preference for nonzero values, but with the opposite sign,

$$[C_{lq}^{(3),22}]^{\text{EW/Higgs}} = (-0.11 \pm 0.06)\,\text{TeV}^{-2}\,. \tag{5.6}$$

This is to be expected, since it is well known that explaining Δ_{CKM} through increasing the muon decay matrix element is in tension with fits in other EWPOs, e.g. see refs. [149–151]. We may yet respect CKM unitarity and decrease the muon decay rate with respect to the SM expectation by breaking LFU, with $0 < C_{Hl}^{(3),22} < -C_{Hl}^{(3),11}$. Let us then allow for nonzero values at the TeV scale for $C_{lq}^{(3),\alpha\alpha}$ for the first two lepton families and also for the corresponding $C_{lq}^{(1),\alpha\alpha}$, typically induced in UV models by the same couplings. The minimum χ^2 follows the expected pattern, plus a preference for $C_{lq}^{(1),11} \approx C_{lq}^{(3),11}$

---

[5]V_{ub} has a completely negligible numerical role in this relation.
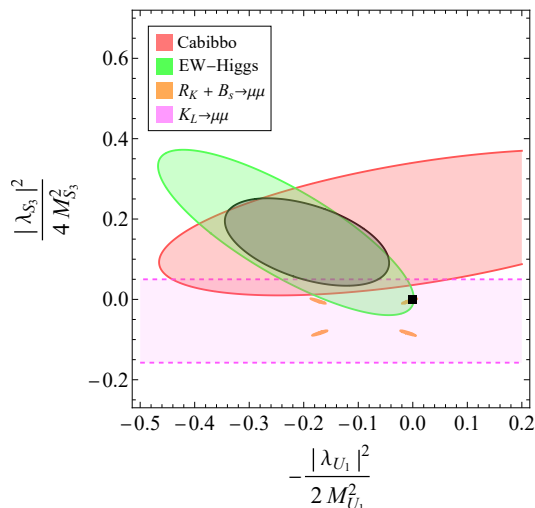
Figure 11. Allowed regions (95 % CL) for the studied leptoquark couplings (see text) from the Cabibbo and the EW Higgs sector and combined, in black. Masses are in TeV units. The preferred nonzero values can be ruled out from B-physics and K-physics observables, unless one defines the top-philic set up in the down-quark basis.

and $C_{lq}^{(1),22} \approx 3C_{lq}^{(3),22}$. Both these relations and the obtained signs happen to match the couplings induced by top-philic U_1 and S_3 leptoquarks coupled, respectively, to the first and the second lepton family,

$$\mathcal{L} \supset \lambda_{U_1} \, \bar{q}_3 \gamma_\mu l_1 \, U_1^\mu + \lambda_{S_3} \, \bar{q}_3^c i\sigma_2 \sigma_a l_2 \, S_3^a + \text{h.c.} \,, \tag{5.7}$$

giving [139, 140]

$$C_{lq}^{(3),11} = -\frac{|\lambda_{U_1}|^2}{2M_{U_1}^2}, \quad C_{lq}^{(3),22} = \frac{|\lambda_{S_3}|^2}{4M_{S_3}^2} \,, \tag{5.8}$$

plus the relations with $C_{lq}^{(1)}$ above. Imposing them as strict equalities one finds, in this two-parameter scenario,

$$C_{lq}^{(3),11} = (-0.19 \pm 0.06) \, \text{TeV}^{-2}, \, C_{lq}^{(3),22} = (0.14 \pm 0.04) \, \text{TeV}^{-2} \,. \tag{5.9}$$

With respect to the SM, this minimum has a $\Delta\chi^2 = 8.0$ preference for the Cabibbo sector and a $\Delta\chi^2 = 5.7$ for the EW/Higgs one.

It is only when adding constraints from B and K physics observables when this scenario becomes strongly disfavored. In a generic top-philic set-up defined in any specific flavor basis in which $C_{lq}^{(1,3),ii}$ are induced, FCNCs are generated when rotating to the mass basis. In the down sector FCNCs are very strongly constrained by the processes studied in this work, as we have explicitly shown when defining the top-philic condition in the up quark basis. Indeed we show in figure 11 how including those constraints we can rule out this, and practically any, top-philic explanation to the Cabibbo anomaly.

Let us finish this section by remarking that there is, however, a possible way out to the strong constraints on FCNCs coming from K and B physics. Assuming that there exists

some, admittedly bizarre from our infra-red perspective, mechanism in the UV theory to select a top-philic set-up in the only basis where this operator does not induce tree-level FCNCs in the down sector, i.e. the down-quark basis, the previous constraints from K and B physics do not hold, while the constraints on Cabibbo angle and EW/Higgs would give, in a first approximation, the same results, since the leading mechanism to modify the SM, through modifying lepton vertices, is largely independent on quark-basis rotation. In that scenario, this leptoquark model may still be a feasible (partial) solution to the Cabibbo anomaly. Complementary constraints on the space of parameters may come from $D - \bar{D}$ mixing (since FCNCs are yet induced in the up sector) and direct leptoquark searches, bounding the possible masses from below. Further studying this scenario is, however, well beyond the goals and the scope of this work.

6 Conclusions

This paper provides a global analysis of indirect constraints on SMEFT operators involving the top quark. In fact, several motivated UV scenarios predict new physics coupled mostly with the top. Our global analysis combines a large number of observables that do not involve directly the top quark. These include: B, K and τ decays, meson mixing observables, magnetic moments of leptons, measurements of the Cabibbo angle, EW precision measurements, Higgs physics, and LFV tests. Top quark operators contribute to these observables either at the tree-level via the $\mathrm{SU}(2)_L$ connection with left-handed down quarks or via loop effects. Assuming that top quark operators are generated at the 1TeV scale, we evolve them down to the scale relevant for each observable using the relevant RG and matching equations. The result of this process is a global likelihood expressed in terms of the high-scale Wilson coefficients.

Using this likelihood we derive global indirect constraints on single coefficients, comparing the result with the bounds obtained from LHC analysis of processes involving top quarks. In all cases we find that the indirect constraints are stronger than the direct ones, often by several orders of magnitude. We then perform several 2D fits to study interesting correlations among coefficients and the complementarity between different observables, that showcase the importance of performing such global analyses. We also perform a multi-dimensional Gaussian fit of all the coefficients of non-leptonic operators, that can be useful to identify the directions in parameter space that have strongest or weakest constraints. Indeed, among these coefficients we identify two almost-flat directions.

Finally, as examples of possible applications of our analysis we study the EFT coefficients generated by two simple UV models. The first includes a scalar singlet leptoquark coupled only to the third generation of quark and lepton doublets. We show how the different indirect constraints one can derive from different sectors combine in providing strong bounds on the model, and how these are complementary to direct searches at the LHC. As a second example we study a two-leptoquark scenario inspired by the Cabibbo anomaly, with only two free couplings. This model accommodates the anomaly and improves the fit quality for the rest of EW-Higgs precision observables. However, B and kaon physics con-

straints are able to completely rule out this scenario unless a very specific flavor alignment is imposed.

Our results show how global indirect constraints on top quark operators can be powerful in constraining new physics scenarios coupled mainly to the top quark. Such constraints are often much stronger, or in any case complementary, to those derived from high-energy top quark physics at colliders. Furthermore, several of the observables providing the strongest indirect constraints are expected to be measured with a substantially better precision in the future: $R^\nu_{K^{(*)}}$ and τ decays at Belle-II, $R_{K^{(*)}}$ and $B_s \to \mu\mu$ by LHCb, ATLAS and CMS, $K \to \pi\nu\nu$ by NA62, and several experiments are expected to improve the sensitivity on $\mu \to e$ LFV by several orders of magnitude. All this will further increase the relevance of such global analysis of indirect bounds in the future.

Acknowledgments

A Observables

A.1 $B \to K^{(*)}\nu\bar{\nu}$ and $K \to \pi\nu\bar{\nu}$

The Standard Model prediction and SMEFT parametrization of dineutrino modes $B \to K^{(*)}\nu\bar{\nu}$ are deeply discussed in ref. [152]. The effective Hamiltonian for these processes reads

$$
\begin{aligned}
\mathcal{H}_{\text{eff}} &= -\frac{4G_F}{\sqrt{2}} \frac{\alpha}{4\pi} \sum_{i,j} V_{ti}^* V_{tj} \left(C_L^{ij\alpha\beta} O_L^{ij\alpha\beta} + C_R^{ij\alpha\beta} O_R^{ij\alpha\beta} \right) \\
&= -\sum_{i,j} \left(\frac{1}{2} L^{V,LL}_{\substack{\nu d \\ \alpha\beta ij}} O_L^{ij\alpha\beta} + \frac{1}{2} L^{V,LR}_{\substack{\nu d \\ \alpha\beta ij}} O_R^{ij\alpha\beta} \right) ,
\end{aligned}
\tag{A.1}
$$

where

$$
O_L^{ij\alpha\beta} = (\bar{d}_i\gamma_\mu P_L d_j)(\bar{\nu}_\alpha \gamma^\mu(1-\gamma_5)\nu_\beta) , \qquad O_R^{ij\alpha\beta} = (\bar{d}_i\gamma_\mu P_R d_j)(\bar{\nu}_\alpha \gamma^\mu(1-\gamma_5)\nu_\beta) . \tag{A.2}
$$

and $L^{V,LL(R)}_{\nu d}$ are LEFT coefficients given in table 15. The ratios

$$
R_K^\nu = \frac{\mathcal{B}(B \to K\nu\bar{\nu})}{\mathcal{B}(B \to K\nu\bar{\nu})_{\text{SM}}} , \qquad R_{K^*}^\nu = \frac{\mathcal{B}(B \to K^*\nu\bar{\nu})}{\mathcal{B}(B \to K^*\nu\bar{\nu})_{\text{SM}}} , \tag{A.3}
$$

can be expressed in terms of two parameters $\epsilon > 0$ and $\eta \in [-1/2, 1/2]$ as:

$$
\begin{aligned}
R_K^\nu &= \sum_{\alpha\beta} \frac{1}{3}(1 - 2\eta_{\alpha,\beta})\epsilon^2_{\alpha\beta} , \qquad R_{K^*}^\nu = \sum_{\alpha\beta} \frac{1}{3}(1 + \kappa_\eta \eta_{\alpha,\beta})\epsilon^2_{\alpha\beta}, \\
\epsilon_{\alpha\beta} &= \frac{\sqrt{|C_{L,\text{SM}}^{sb}\delta_{\alpha\beta} + C_L^{sb\alpha\beta}|^2 + |C_R^{sb\alpha\beta}|^2}}{|C_{L,\text{SM}}^{sb}|} , \\
\eta_{\alpha\beta} &= -\frac{\text{Re}\left[\left(C_{L,\text{SM}}^{sb}\delta_{\alpha\beta} + C_L^{sb\alpha\beta}\right)\left(C_R^{sb\alpha\beta}\right)^* \right]}{|C_{L,\text{SM}}^{sb}\delta_{\alpha\beta} + C_L^{sb\alpha\beta}|^2 + |C_R^{sb\alpha\beta}|^2} ,
\end{aligned}
\tag{A.4}
$$

where the parameter κ_η depends on form factors. There are not isospin asymmetries between the charged and neutral meson decays to neutrinos, so that the only difference between $\mathcal{B}(B^\pm \to K^{\pm(*)}\nu\bar\nu)$ and $\mathcal{B}(B^0 \to K^{0(*)}\nu\bar\nu)$ is in the lifetime $\tau_{B^\pm}$ and τ_{B^0}, that cancel in the ratio. Remarkably, in our setup the coefficient C_R is zero at the level of dimension-six SMEFT contributions, so that $\eta_{\alpha\beta} = 0$ and then the theoretical predictions for R_K^ν and $R_{K^*}^\nu$ coincide.

For kaons, we use directly the branching ratios. Since $C_R = 0$ in our setup, we can just write them in terms of the SM values rescaling the C_L coefficients

$$
\begin{aligned}
\mathcal{B}(K^+ \to \pi^+ \nu\bar\nu)_{th} &= \mathcal{B}(K^+ \to \pi^+ \nu_e \bar\nu_e)_{\text{SM}} \sum_{\alpha,\beta=1,2} \left| \delta_{\alpha\beta} + \frac{C_L^{ds\alpha\beta}}{C_{L,\text{SM}}^{ds11}} \right|^2 \\
&+ \mathcal{B}(K^+ \to \pi^+ \nu_\tau \bar\nu_\tau)_{\text{SM}} \left[\left| 1 + \frac{C_L^{ds33}}{C_{L,\text{SM}}^{ds33}} \right|^2 + \sum_{\alpha=1,2} \left(\left| \frac{C_L^{ds\alpha3}}{C_{L,\text{SM}}^{ds33}} \right|^2 + \left| \frac{C_L^{ds3\alpha}}{C_{L,\text{SM}}^{ds33}} \right|^2 \right) \right] ,
\end{aligned}
\tag{A.5}
$$

$$
\begin{aligned}
\mathcal{B}(K_L \to \pi^0 \nu\bar\nu)_{th} &= \frac{1}{3}\mathcal{B}(K_L \to \pi^0 \nu\bar\nu)_{\text{SM}} \left[\sum_{\alpha,\beta=1,2} \left(\delta_{\alpha\beta} + \frac{\text{Im}[N_{ds}^{-1}C_L^{ds\alpha\beta}]}{\text{Im}[N_{ds}^{-1}C_{L,\text{SM}}^{ds11}]} \right)^2 \right. \\
&+ \left. \left(1 + \frac{\text{Im}[N_{ds}^{-1}C_L^{ds33}]}{\text{Im}[N_{ds}^{-1}C_{L,\text{SM}}^{ds33}]} \right) + \sum_{\alpha=1,2} \left(\left(\frac{\text{Im}[N_{ds}^{-1}C_L^{ds\alpha3}]}{\text{Im}[N_{ds}^{-1}C_{L,\text{SM}}^{ds33}]} \right) + \left(\frac{\text{Im}[N_{ds}^{-1}C_L^{ds3\alpha}]}{\text{Im}[N_{ds}^{-1}C_{L,\text{SM}}^{ds33}]} \right) \right) \right] ,
\end{aligned}
\tag{A.6}
$$

where we defined $N_{ds} = (\sqrt{2}G_F \alpha V_{td}^* V_{ts}/\pi)^{-1}$ and the SM values for the branching ratios and Wilson coefficients are

$$
\begin{aligned}
\mathcal{B}(K^+ \to \pi^+ \nu_e \bar\nu_e)_{\text{SM}} &= 3.06 \times 10^{-11} , \\
\mathcal{B}(K^+ \to \pi^+ \nu_\tau \bar\nu_\tau)_{\text{SM}} &= 2.52 \times 10^{-11} , \\
\mathcal{B}(K_L \to \pi^0 \nu\bar\nu)_{\text{SM}} &= 3.4 \times 10^{-11} ,
\end{aligned}
\tag{A.7}
$$

$$
C_{L,\text{SM}}^{ds\alpha\beta} = -\frac{1}{s_W^2}\left(X_t + \frac{V_{cd}^* V_{cs}}{V_{td}^* V_{ts}} X_c^\alpha \right) \delta_{\alpha\beta} ,
\tag{A.8}
$$

with $X_\tau = 1.481$, $X_c^e = X_c^\mu = 1.053 \times 10^{-3}$ and $X_c^t = 0.711 \times 10^{-3}$.

A.2 $B_s \to \ell_\alpha^- \ell_\beta^+$ and $K_{L,S} \to \ell_\alpha^- \ell_\beta^+$

The branching ratio for rare leptonic B decays is discussed, for example, in ref. [153] and the same description holds also for kaons. In our framework, these processes are induced by the operators

$$
O_9^{ij\alpha\beta} = (\bar d_i \gamma_\mu P_L d_j)(\bar\ell_\alpha \gamma^\mu \ell_\beta) , \quad O_{10}^{ij\alpha\beta} = (\bar d_i \gamma_\mu P_L d_j)(\bar\ell_\alpha \gamma^\mu \gamma_5 \ell_\beta) ,
\tag{A.9}
$$

appearing in the effective Hamiltonian

$$
\mathcal{H}_{\text{eff}} = -\frac{4G_F}{\sqrt{2}}\frac{\alpha}{4\pi} \sum_{k=9,10} V_{ti}^* V_{tj} \mathcal{C}_k^{ij\alpha\beta} \mathcal{O}_k^{ij\alpha\beta} .
\tag{A.10}
$$

We do not take into account the other possible contributions: the operators $O_{9',10'}$, with $P_L \to P_R$, are identically zero in our setup and we do not consider the usual scalar and

pseudoscalar operators O_S and O_P (see e.g. in ref. [153]), since they are generated with negligible coefficients with respect to O_9 and O_{10}. The relation between these coefficients and the LEFT ones is

$$C_{9(10)}^{ij\alpha\beta} = \frac{\sqrt{2}\pi}{G_F \alpha V_{ti}^* V_{tj}} \left(L_{\substack{de \\ ij\alpha\beta}}^{V,LR} \pm L_{\substack{ed \\ \alpha\beta ij}}^{V,LL} \right) . \tag{A.11}$$

The branching ratio for the leptonic B_s decays is given by

$$\mathcal{B}(B_s \to \ell_\alpha^- \ell_\beta^+)_{th} = \frac{\tau_{B_s}}{64\pi^3} \frac{\alpha^2 G_F^2}{m_{B_s}^3} f_{B_s}^2 |V_{tb} V_{ts}^*|^2 \lambda^{1/2}(m_{B_s}, m_\alpha, m_\beta) \times$$

$$\times \left[\left[m_{B_s}^2 - (m_\alpha + m_\beta)^2 \right] \times \left| (C_{9,\text{SM}}^{sb\alpha\beta} + C_9^{sb\alpha\beta})(m_\alpha - m_\beta) \right|^2 + \tag{A.12} \right.$$

$$\left. + \left[m_{B_s}^2 - (m_\alpha - m_\beta)^2 \right] \times \left| (C_{10,\text{SM}}^{sb\alpha\beta} + C_{10}^{sb\alpha\beta})(m_\alpha + m_\beta) \right|^2 \right],$$

where $\lambda(a, b, c) = [a^2 - (b - c)^2][a^2 - (b + c)^2]$. When comparing the theoretical prediction of B decays to untagged experimental data, the sizeable decay width differences in the $B_s^0 - \bar{B}_s^0$ system must be taken into account. This is done by using an effective lifetime. To a good approximation one has [154, 155]

$$\mathcal{B}(B_s \to \ell_\alpha^- \ell_\beta^+)_{\text{eff}} \simeq \frac{1}{1 - y_s} \mathcal{B}(B_s \to \ell_\alpha^- \ell_\beta^+)_{\text{th}} , \tag{A.13}$$

with $y_s = \Delta\Gamma_{B_s}/(2\Gamma_{B_s}) = 0.064(4)$, according to the current PDG and HFLAV average [38]. Numerical values for couplings and parameters appearing in the formula can be found in refs. [38, 156]. The expression in eq. (A.12) can be applied to $B_d \to \ell_\alpha^- \ell_\beta^+$ with the obvious $s \to d$ replacement.

The leptonic kaon decays are instead given by

$$\mathcal{B}(K_{L(S)} \to \ell_\alpha^- \ell_\beta^+)_{th} = \frac{\tau_{K_L}}{128\pi^3} \frac{\alpha^2 G_F^2}{m_{K_0}^3} f_K^2 |V_{td} V_{ts}^*|^2 \lambda^{1/2}(m_K, m_\alpha, m_\beta) \times$$

$$\times \left[\left[m_{K_0}^2 - (m_\alpha + m_\beta)^2 \right] \times \left| \left(C_{9,\text{SM}}^{ds\alpha\beta} \pm C_{9,\text{SM}}^{sd\alpha\beta} + C_9^{ds\alpha\beta} \pm C_9^{sd\alpha\beta} \right) \right|^2 (m_\alpha - m_\beta)^2 + \right.$$

$$\left. + \left[m_{K_0}^2 - (m_\alpha - m_\beta)^2 \right] \times \left| \left(C_{10,\text{SM}}^{ds\alpha\beta} \pm C_{10,\text{SM}}^{sd\alpha\beta} + C_{10}^{ds\alpha\beta} \pm C_{10}^{sd\alpha\beta} \right) \right|^2 (m_\alpha + m_\beta)^2 \right]. \tag{A.14}$$

Notice that for kaons both ds and sd indices appear, since $K_{L,S}$ are linear combinations of K^0 and $\bar{K}^0$

$$\left| K_{L(S)} \right\rangle = \frac{\left| K^0 \right\rangle \pm \left| \bar{K}^0 \right\rangle}{\sqrt{2}} . \tag{A.15}$$

In all cases, as one can expect, for $\ell_\alpha = \ell_\beta = \ell$ the coefficient C_9 does not contribute.

A.3 $B \to K^{(*)}\ell^+\ell^-$

In ref. [157], the leading contributions to the decay width of $B \to K^{(*)}\ell^+\ell^-$ are computed. Under some justified assumptions, the R_K and R_{K^*} ratios read

$$
\begin{aligned}
R_K([1.1, 6]) \approx &1.00 + 0.24\text{Re}[C_9 - C_{10}] + 0.24\text{Re}[C_9' - C_{10}'] + 0.058\text{Re}[C_9^* C_9' + \\
&+ C_{10}^* C_{10}'] + 0.029\left(|C_9|^2 + |C_9'|^2 + |C_{10}|^2 + |C_{10}'|^2\right), \\
R_{K^*}([1.1, 6]) \approx &1.00 + 0.24\text{Re}[C_9 - C_{10}] - 0.18\text{Re}[C_9'] + 0.17\text{Re}[C_{10}'] - 0.042\text{Re}[C_9^* C_9' + \\
&+ C_{10}^* C_{10}'] + +0.029\left(|C_9|^2 + |C_9'|^2 + |C_{10}|^2 + |C_{10}'|^2\right),
\end{aligned}
$$

where the operators and the Hamiltonian are defined as in appendix A.9–A.10. The numerical coefficients are compatible with the ones computed, for example, in refs. [158–160] and with our calculation of R_{K^*}, derived using expressions and form factors provided in refs. [161, 162]. The primed coefficients C_9' and C_{10}' are displayed for completeness, but they are anyway set to zero as they are not generated by the operators in table 1.

A.4 $K_L \to \pi^0 \ell^+ \ell^-$

We consider again the Hamiltonian in eq. (A.10) and we define $\tilde{C}_k^{ij\alpha\beta} = V_{ti}^* V_{tj} C_k^{ij\alpha\beta}$. Rearranging the formula given in ref. [163] to fit our notation, we obtain for the branching ratio

$$
\mathcal{B}(K_L \to \pi^0 \ell^+ \ell^-)_{th} = a_\ell\left[(\omega_{7V}^\ell)^2 + (\omega_{7A}^\ell)^2\right] + b_\ell \omega_{7V}^\ell + c_\ell, \tag{A.16}
$$

where

$$
\begin{aligned}
\omega_{7V}^\ell &= \frac{1}{2\pi}\frac{1}{1.407 \times 10^{-4}}\left[P_0\text{Im}(V_{ts}^* V_{td}) + \text{Im}(C_{9,\text{SM}}^{sd\ell\ell} + C_9^{sd\ell\ell})\right], \\
\omega_{7A}^\ell &= \frac{1}{2\pi}\frac{1}{1.407 \times 10^{-4}}\text{Im}(C_{10,\text{SM}}^{sd\ell\ell} + C_{10}^{sd\ell\ell}).
\end{aligned}
\tag{A.17}
$$

The numerical coefficients a, b and c are given by

$$
\begin{aligned}
a_e &= 4.62 \times 10^{-12}, & a_\mu &= 1.09 \times 10^{-12}, \\
b_e &= 13.56 \times 10^{-12}, & b_\mu &= 3.156 \times 10^{-12}, \\
c_e &= 20.88 \times 10^{-12}, & c_\mu &= 10.0384 \times 10^{-12}.
\end{aligned}
\tag{A.18}
$$

A.5 $P \to M\ell_\alpha^- \ell_\beta^+$

We consider here the semileptonic decay of a meson $P = \{B, K_L, K^+\}$ into $M = \{K^{(*)}, \pi\}$ and two different leptons. The branching ratios for the decays are [153, 164]

$$
\mathcal{B}(P \to M\ell_\alpha^- \ell_\beta^+)_{th} = \frac{1}{8G_F^2}\left(\alpha_V^+ \left|L_{\substack{de \\ ij\alpha\beta}}^{V,LR} + L_{\substack{ed \\ \alpha\beta ij}}^{V,LL}\right|^2 + \alpha_V^- \left|L_{\substack{de \\ ij\alpha\beta}}^{V,LR} - L_{\substack{ed \\ \alpha\beta ij}}^{V,LL}\right|^2\right). \tag{A.19}
$$

Numerical values for the multiplicative coefficients are given in table 13. The indices ij correspond to the transition $q_j \to q_i \ell_\alpha^- \ell_\beta^+$ and for K_L it is understood the average $(ds + sd)/2$.

Process	α_V^+	α_V^-
$B \to K e^+ \mu^-$	8.2(6)	8.2(6)
$B \to K e^+ \tau^-$	5.3(2)	5.3(2)
$B \to K \mu^+ \tau^-$	5.2(2)	5.2(2)
$B \to K^* e^+ \mu^-$	2.8(5)	2.8(5)
$B \to K^* e^+ \tau^-$	1.4(2)	1.4(2)
$B \to K^* \mu^+ \tau^-$	1.5(2)	1.3(2)
$K^+ \to \pi^+ e^+ \mu^-$	0.596(4)	0.598(4)
$K_L \to \pi^0 e^+ \mu^-$	2.75(2)	2.76(2)

Table 13. Values for the factors defined in eq. (A.19), for all the possible final states. Details on their computation can be found in ref. [164].

A.6 $B \to X_s \gamma$

The inclusive radiative B decays can be parametrized in terms of the operators

$$O_7 = \frac{e}{16\pi^2} m_b(\bar{s}\sigma_{\alpha\beta}P_{R(L)}b)F^{\alpha\beta}\,, \quad O_8 = \frac{g}{16\pi^2} m_b(\bar{s}\sigma_{\alpha\beta}P_{R(L)}T^a b)G_a^{\alpha\beta}\,, \tag{A.20}$$

and the effective Hamiltonian

$$\mathcal{H}_{\text{eff}} = -\frac{4G_F}{\sqrt{2}}V_{ts}^*V_{tb}\sum_i \mathcal{C}_i\mathcal{O}_i\,. \tag{A.21}$$

The branching ratio is given then by [165, 166]

$$\mathcal{B}(\bar{B} \to X_s\gamma)_{E_\gamma > 1.6\,\text{GeV}} = 10^{-4} \times (3.36 \pm 0.23 - 8.22C_7 - 1.99C_8)\,, \tag{A.22}$$

where the coefficients are defined at the matching scale $\mu_0 = 160\,\text{GeV}$ [165]. In terms of LEFT coefficients, we have:

$$\begin{aligned}
C_7 &= \frac{N_{sb}^{-1}e}{m_b} \times L_{d\gamma}\,, \qquad C_8 = \frac{N_{sb}^{-1}e^2}{gm_b}L_{dG}\,, \\
N_{sb} &= \frac{4G_F}{\sqrt{2}}\frac{\alpha_{em}}{4\pi}V_{ts}^*V_{tb}\,.
\end{aligned} \tag{A.23}$$

A.7 Charged lepton flavor violation

For charged lepton flavour violation processes we employ the expressions from refs. [112, 117], after translating them to the LEFT basis. In the following we give the explicit expressions used in this work.

- $\ell_H \to \ell_L \gamma$

  We may take a reference renormalization scale $\mu = 2\,\text{GeV}$, where the LEFT is yet well defined. One has [112, 117, 167]

$$\Gamma_{\ell \to \ell'\gamma} = \frac{m_\ell^3}{4\pi}[|L_{e\gamma}|^2 + |L_{e\gamma}|^2]\,. \tag{A.24}$$

The (nonperturbative) effect of four-fermion operators involving tensor light-quark currents can be taken into account by making the following transformations

$$L_{\substack{e\gamma \\ \ell'\ell}} \to L_{\substack{e\gamma \\ \ell'\ell}} - e\left(c_3^{\ell'\ell} + \frac{c_8^{\ell'\ell}}{\sqrt{3}}\right)i\Pi_{VT}(0)\,, \tag{A.25}$$

$$L_{\substack{e\gamma \\ \ell\ell'}} \to L_{\substack{e\gamma \\ \ell\ell'}} + e\left(c_3^{\ell\ell'} + \frac{c_8^{\ell\ell'}}{\sqrt{3}}\right)i\Pi_{VT}(0)\,, \tag{A.26}$$

with

$$c_3^{ij} = L_{\substack{eu \\ ij11}}^{T,RR} - L_{\substack{ed \\ ij11}}^{T,RR}\,, \tag{A.27}$$

$$c_8^{ij} = \frac{1}{\sqrt{3}}\left[L_{\substack{eu \\ ij11}}^{T,RR} + L_{\substack{ed \\ ij11}}^{T,RR} - 2L_{\substack{ed \\ ij22}}^{T,RR}\right]\,. \tag{A.28}$$

As in ref. [117] we take $i\Pi_{VT}(0) \approx 0.04\,\mathrm{GeV}$.

- $\tau \to 3e$, $\tau \to 3\mu$, $\mu \to 3e$

  We use the analytic expressions given in ref. [117], adapting them to the LEFT normalization of this work. Numerically we find, in GeV units,

$$\begin{aligned}
\mathcal{B}(\tau \to 3e) \approx{}& 1.6 \times 10^8 (|L_{\substack{ee \\ 1113}}^{S,RR}|^2 + |L_{\substack{ee \\ 1113}}^{V,LR}|^2 + |L_{\substack{ee \\ 1311}}^{V,LR}|^2) \\
& + 1.3 \times 10^9 (|L_{\substack{ee \\ 1311}}^{V,LL}|^2 + |L_{\substack{ee \\ 1311}}^{V,RR}|^2) + 2.1 \times 10^9 (|L_{\substack{e\gamma \\ 31}}|^2 + |L_{\substack{e\gamma \\ 13}}|^2) \\
& + [L_{\substack{e\gamma \\ 31}}(-4.5 \times 10^8 L_{\substack{ee \\ 1113}}^{V,LL} - 1.1 \times 10^8 L_{\substack{ee \\ 1311}}^{V,LR}) + c.c.] \\
& + [L_{\substack{e\gamma \\ 13}}^*(-4.5 \times 10^8 L_{\substack{ee \\ 1113}}^{V,RR} - 1.1 \times 10^8 L_{\substack{ee \\ 1113}}^{V,LR}) + c.c.]\,. \tag{A.29}
\end{aligned}$$

The analytic expressions trivially generalize for $\tau \to 3\mu$, $\mu \to 3e$. Numerically one finds

$$\begin{aligned}
\mathcal{B}(\tau \to 3\mu) \approx{}& 1.6 \times 10^8 (|L_{\substack{ee \\ 1123}}^{S,RR}|^2 + |L_{\substack{ee \\ 1123}}^{V,LR}|^2 + |L_{\substack{ee \\ 2311}}^{V,LR}|^2) \\
& + 1.3 \times 10^9 (|L_{\substack{ee \\ 2311}}^{V,LL}|^2 + |L_{\substack{ee \\ 2311}}^{V,RR}|^2) + 4.4 \times 10^8 (|L_{\substack{e\gamma \\ 32}}|^2 + |L_{\substack{e\gamma \\ 23}}|^2) \\
& + [L_{\substack{e\gamma \\ 32}}(-4.5 \times 10^8 L_{\substack{ee \\ 1123}}^{V,LL} - 1.1 \times 10^8 L_{\substack{ee \\ 2311}}^{V,LR}) + c.c.] \\
& + [L_{\substack{e\gamma \\ 23}}^*(-4.5 \times 10^8 L_{\substack{ee \\ 1123}}^{V,RR} - 1.1 \times 10^8 L_{\substack{ee \\ 1123}}^{V,LR}) + c.c.]\,, \tag{A.30}
\end{aligned}$$

and

$$\begin{aligned}
\mathcal{B}(\mu \to 3e) \approx{}& 9.2 \times 10^8 (|L_{\substack{ee \\ 1112}}^{S,RR}|^2 + |L_{\substack{ee \\ 1112}}^{V,LR}|^2 + |L_{\substack{ee \\ 1211}}^{V,LR}|^2) \\
& + 7.4 \times 10^9 (|L_{\substack{ee \\ 1211}}^{V,LL}|^2 + |L_{\substack{ee \\ 1211}}^{V,RR}|^2) + 1.9 \times 10^{12} (|L_{\substack{e\gamma \\ 21}}|^2 + |L_{\substack{e\gamma \\ 12}}|^2) \\
& + [L_{\substack{e\gamma \\ 21}}(-4.2 \times 10^{10} L_{\substack{ee \\ 1112}}^{V,LL} - 1.1 \times 10^{10} L_{\substack{ee \\ 1211}}^{V,LR}) + c.c.] \\
& + [L_{\substack{e\gamma \\ 12}}^*(-4.2 \times 10^{10} L_{\substack{ee \\ 1112}}^{V,RR} - 1.1 \times 10^{10} L_{\substack{ee \\ 1112}}^{V,LR}) + c.c.]\,, \tag{A.31}
\end{aligned}$$

- $\tau \to e\bar{\mu}\mu$, $\tau \to \mu\bar{e}e$.

  Once again we adapt the analytic results as given in ref. [117], finding

  $$
  \begin{aligned}
  \mathcal{B}(\tau \to e\bar{\mu}\mu) \approx\ & 2.5 \times 10^9 (|L^{V,LL}_{\underset{1223}{ee}}|^2 + |L^{V,RR}_{\underset{1223}{ee}}|^2) \\
  & + 1.6 \times 10^8 (|L^{V,LR}_{\underset{2213}{ee}}|^2 + |L^{V,LR}_{\underset{1322}{ee}}|^2) + 1.0 \times 10^8 (|L_{\underset{31}{e\gamma}}|^2 + |L_{\underset{13}{e\gamma}}|^2) \\
  & - 2.1 \times 10^8 [L_{\underset{31}{e\gamma}} L^{V,LL}_{\underset{1223}{ee}} + c.c.] \\
  & + [L^*_{\underset{13}{e\gamma}}(-5.2 \times 10^7 L^{*V,LR}_{\underset{1322}{ee}} - 2.6 \times 10^8 L^{V,RR}_{\underset{1223}{ee}}) + c.c.]\,, \quad (A.32)
  \end{aligned}
  $$

  and

  $$
  \begin{aligned}
  \mathcal{B}(\tau \to \mu\bar{e}e) \approx\ & 2.6 \times 10^9 (|L^{V,LL}_{\underset{1123}{ee}}|^2 + |L^{V,RR}_{\underset{1123}{ee}}|^2) \\
  & + 1.6 \times 10^8 (|L^{V,LR}_{\underset{1123}{ee}}|^2 + |L^{V,LR}_{\underset{2311}{ee}}|^2) + 5.0 \times 10^8 (|L_{\underset{32}{e\gamma}}|^2 + |L_{\underset{23}{e\gamma}}|^2) \\
  & - 2.2 \times 10^8 [L_{\underset{32}{e\gamma}} L^{V,LL}_{\underset{1123}{ee}} + c.c.] \\
  & + [L^*_{\underset{23}{e\gamma}}(-5.5 \times 10^7 L^{*V,LR}_{\underset{2311}{ee}} - 2.8 \times 10^8 L^{V,RR}_{\underset{1123}{ee}}) + c.c.]\,. \quad (A.33)
  \end{aligned}
  $$

- $\mu\mathrm{Au} \to e\mathrm{Au}$.

  We adapt the results of ref. [112], neglecting the power-suppressed contributions from c and b quarks. In principle they are given at a $\mu = 1\,\mathrm{GeV}$, but within the theoretical uncertainties the same expressions can also be used at $\mu = 2\,\mathrm{GeV}$.[6] We have also checked that we agree with the adaptation given in ref. [167]. The numerical result is rather large. For reference, the first quadratic coefficients are

  $$
  \mathcal{B}(\mu\mathrm{Au} \to e\mathrm{Au}) \approx 1.1 \times 10^{13} [(L^{S,RL}_{\underset{1211}{ed}})^2 + (L^{S,RL}_{\underset{2111}{ed}})^2 + (L^{S,RR}_{\underset{2111}{ed}})^2 + (L^{S,RR}_{\underset{1211}{ed}})^2 + (d \to u)]
  $$
  $$(A.34)$$

- $\tau \to \ell\pi^0$

  We take the numerical result of ref. [117]. Adapting it to the normalization of this work we have

  $$
  \begin{aligned}
  \mathcal{B}(\tau \to \ell\pi^0) \approx\ & 1.3 \times 10^8 |L^{S,RL}_{\underset{\ell311}{ed}} - L^{S,RL}_{\underset{\ell311}{eu}} - L^{S,RR}_{\underset{\ell311}{ed}} + L^{S,RR}_{\underset{\ell311}{eu}}|^2 \\
  & + 5.1 \times 10^7 |L^{V,LL}_{\underset{3\ell11}{ed}} - L^{V,LL}_{\underset{3\ell11}{eu}} - L^{V,LR}_{\underset{3\ell11}{ed}} + L^{V,LR}_{\underset{3\ell11}{eu}}|^2\,. \quad (A.35)
  \end{aligned}
  $$

- $\tau \to \ell\pi^+\pi^-$

  Once again we use the numerical results from ref. [117]. We find

  $$
  \begin{aligned}
  \mathcal{B}(\tau \to \ell\pi\pi) \approx\ & 9.2 \times 10^8 |L^{T,RR}_{\underset{3\ell11}{ed}} - L^{T,RR}_{\underset{3\ell11}{eu}}|^2 + 4.6 \times 10^8 |L^{V,LL}_{\underset{3\ell11}{ed}} - L^{T,LL}_{\underset{3\ell11}{eu}} + L^{V,LR}_{\underset{3\ell11}{ed}} - L^{T,LR}_{\underset{3\ell11}{eu}}|^2 \\
  & + 5.0 \times 10^8 |L_{\underset{3\ell}{e\gamma}}|^2 + 1.6 \times 10^8 |L^{S,RL}_{\underset{3\ell11}{ed}} + L^{S,RL}_{\underset{3\ell11}{eu}} + L^{S,RR}_{\underset{3\ell11}{ed}} + L^{S,RR}_{\underset{3\ell11}{eu}}|^2 \\
  & + 1.2 \times 10^8 |L^{S,RL}_{\underset{3\ell22}{ed}} + L^{S,RR}_{\underset{3\ell11}{ed}}|^2\,. \quad (A.36)
  \end{aligned}
  $$

---

[6]The large QCD running of the scalar quark current is fully taken into account by simply taking as input $m_q(\mu = 2\,\mathrm{GeV})$ instead of $m_q(\mu = 1\,\mathrm{GeV})$.

$\tau \to \ell\eta, \tau \to \ell\eta', \tau \to \ell K, \tau \to \ell\pi K, \tau \to \ell K K$ are also included in our χ^2, adapting the compilation of ref. [117]. However they play a marginal phenomenological role in our analysis and thus we refrain from giving the explicit expressions.

A.8 Matching relations for the Cabibbo angle observables

The running of the chirality-flipping low-energy couplings to the M_Z mass is large and needs to be taken into account. From ref. [168], which includes higher-order QCD running effects, one has

$$
\begin{pmatrix} \epsilon_S \\ \epsilon_P \\ \epsilon_T \end{pmatrix}_{\mu=2\,\mathrm{GeV}} = \begin{pmatrix} 1.72 & 2.46 \times 10^{-6} & -0.0242 \\ 2.46 \times 10^{-6} & 1.72 & -0.0242 \\ -2.17 \times 10^{-4} & -2.17 \times 10^{-4} & 0.825 \end{pmatrix} \begin{pmatrix} \epsilon_S \\ \epsilon_P \\ \epsilon_T \end{pmatrix}_{\mu=M_Z} . \tag{A.37}
$$

At M_Z at tree-level one has

$$
-\frac{2\hat{V}_{ud}}{v^2}\epsilon_L^{dse} = 2\left(C^{(3)}_{\substack{Hl \\ 22}} - C^{(3)}_{\substack{Hq \\ 11}} - C_{\substack{ll \\ 1221}} + C^{(3)}_{\substack{lq \\ 1111}} \right)
$$

$$
-\frac{2\hat{V}_{ud}}{v^2}\epsilon_L^{d\ell'/\ell} = L^{V,LL}_{\substack{\nu e du \\ \ell'\ell'11}} - L^{V,LL}_{\substack{\nu e du \\ \ell\ell 11}} = 2V_{ud}(C^{(3)}_{\substack{Hl \\ \ell\ell}} - C^{(3)}_{\substack{Hl \\ \ell'\ell'}} - C^{(3)}_{\substack{lq \\ \ell\ell 11}} + C^{(3)}_{\substack{lq \\ \ell'\ell'11}}) - 2V_{us}(-C^{(3)}_{\substack{lq \\ \ell\ell 21}} + C^{(3)}_{\substack{lq \\ \ell'\ell'21}}) ,
$$

$$
-\frac{2\hat{V}_{us}}{v^2}\epsilon_L^{s\ell'/\ell} = L^{V,LL}_{\substack{\nu e du \\ \ell'\ell'21}} - L^{V,LL}_{\substack{\nu e du \\ \ell\ell 21}} = 2V_{us}(C^{(3)}_{\substack{Hl \\ \ell\ell}} - C^{(3)}_{\substack{Hl \\ \ell'\ell'}} - C^{(3)}_{\substack{lq \\ \ell\ell 11}} + C^{(3)}_{\substack{lq \\ \ell'\ell'11}}) + 2V_{ud}(-C^{(3)}_{\substack{lq \\ \ell\ell 21}} + C^{(3)}_{\substack{lq \\ \ell'\ell'21}}) ,
$$

$$
-\frac{2\hat{V}_{uD}}{v^2}\epsilon_R^D = L^{V,LR}_{\substack{\nu e du \\ \ell\ell D1}} = -C_{\substack{Hud \\ 1D}} ,
$$

$$
-\frac{2\hat{V}_{ud}}{v^2}\epsilon_S^{d\ell} = L^{S,RR}_{\substack{\nu e du \\ \ell\ell 11}} + L^{S,RL}_{\substack{\nu e du \\ \ell\ell 11}} = C_{\substack{ledq \\ \ell\ell 11}} + V_{ud}C^{(1)}_{\substack{lequ \\ \ell\ell 11}} - V_{us}C^{(1)}_{\substack{lequ \\ \ell\ell 21}} ,
$$

$$
-\frac{2\hat{V}_{us}}{v^2}\epsilon_S^{s\ell} = L^{S,RR}_{\substack{\nu e du \\ \ell\ell 21}} + L^{S,RL}_{\substack{\nu e du \\ \ell\ell 21}} = C_{\substack{ledq \\ \ell\ell 21}} + V_{us}C^{(1)}_{\substack{lequ \\ \ell\ell 11}} + V_{ud}C^{(1)}_{\substack{lequ \\ \ell\ell 21}} , \tag{A.38}
$$

$$
-\frac{2\hat{V}_{ud}}{v^2}\epsilon_P^{d\ell} = L^{S,RR}_{\substack{\nu e du \\ \ell\ell 11}} - L^{S,RL}_{\substack{\nu e du \\ \ell\ell 11}} = -C_{\substack{ledq \\ \ell\ell 11}} + V_{ud}C^{(1)}_{\substack{lequ \\ \ell\ell 11}} - V_{us}C^{(1)}_{\substack{lequ \\ \ell\ell 21}} ,
$$

$$
-\frac{2\hat{V}_{us}}{v^2}\epsilon_P^{s\ell} = L^{S,RR}_{\substack{\nu e du \\ \ell\ell 21}} - L^{S,RL}_{\substack{\nu e du \\ \ell\ell 21}} = -C_{\substack{ledq \\ \ell\ell 21}} + V_{us}C^{(1)}_{\substack{lequ \\ \ell\ell 11}} + V_{ud}C^{(1)}_{\substack{lequ \\ \ell\ell 21}} ,
$$

$$
-\frac{2\hat{V}_{ud}}{v^2}\frac{1}{4}\hat{\epsilon}_T^{d\ell} = L^{T,RR}_{\substack{\nu e du \\ \ell\ell 11}} = V_{ud}C^{(3)}_{\substack{lequ \\ \ell\ell 11}} - V_{us}C^{(3)}_{\substack{lequ \\ \ell\ell 21}} ,
$$

$$
-\frac{2\hat{V}_{us}}{v^2}\frac{1}{4}\hat{\epsilon}_T^{s\ell} = L^{T,RR}_{\substack{\nu e du \\ \ell\ell 21}} = V_{us}C^{(3)}_{\substack{lequ \\ \ell\ell 11}} + V_{ud}C^{(3)}_{\substack{lequ \\ \ell\ell 21}} .
$$

The leading mechanism to generate a top operator is through the large mixing of $C^{(3)}_{\substack{Hl \\ \alpha\alpha}}$ with $C^{(3)}_{\substack{lq \\ \alpha\alpha 33}}$ through a double top-Yukawa insertion [20],[7]

$$
v^2 C^{(3)}_{\substack{Hl \\ \alpha\alpha}}(M_Z^2) \approx v^2 4 N_c \frac{m_t^2}{(4\pi v)^2} C^{(3)}_{\substack{lq \\ \alpha\alpha 33}}(\Lambda_{\mathrm{UV}}^2) \log\frac{\Lambda_{\mathrm{UV}}}{M_Z} = \left[\frac{N_c}{4\pi^2} \frac{m_t^2}{\Lambda_{\mathrm{UV}}^2} \log\frac{\Lambda_{\mathrm{UV}}}{M_Z} \right] \Lambda_{\mathrm{UV}}^2 C^{(3)}_{\substack{lq \\ \alpha\alpha 33}}(\Lambda_{\mathrm{UV}}^2) . \tag{A.39}
$$

---

[7]As in the rest of this work, the DSixTools package has been used to perform the full one-loop running. We have also checked that the loop-induced top operators in the SMEFT-LEFT matching play a marginal role in this sector and, in first approximation, can be neglected.

A.9 Higgs basis used for EWPT and Higgs fit

The fit performed in ref. [121] employs a specific combinations of Wilson coefficients of the Warsaw basis, called *Higgs basis*. This allows to reduce the correlations between the directions mostly constrained by EW precision data and those constrained by Higgs data, which differ strongly in the precision. The combinations used are the following:

$$
\begin{aligned}
\delta g_L^{W\ell} &= C_{Hl}^{(3)} + f(1/2, 0) - f(-1/2, -1), \\
\delta g_L^{Z\ell} &= -\frac{1}{2}C_{Hl}^{(3)} - \frac{1}{2}C_{Hl}^{(1)} + f(-1/2, -1), \\
\delta g_R^{Z\ell} &= -\frac{1}{2}C_{He}^{(1)} + f(0, -1), \\
\delta g_L^{Zu} &= \frac{1}{2}C_{Hq}^{(3)} - \frac{1}{2}C_{Hq}^{(1)} + f(1/2, 2/3), \\
\delta g_L^{Zd} &= -\frac{1}{2}C_{Hq}^{(3)} - \frac{1}{2}C_{Hq}^{(1)} + f(-1/2, -1/3), \\
\delta g_R^{Zu} &= -\frac{1}{2}C_{Hu} + f(0, 2/3), \\
\delta g_R^{Zd} &= -\frac{1}{2}C_{Hd} + f(0, -1/3), \\
\delta c_z &= C_{H\Box} - \frac{1}{4}C_{HD} - \frac{3}{2}\Delta_{G_F}, \\
c_{z\Box} &= \frac{1}{2g_L^2}\left(C_{HD} + 2\Delta_{G_F}\right), \\
c_{gg} &= \frac{4}{g_s^2}C_{HG}, \\
c_{\gamma\gamma} &= 4\left(\frac{1}{g_L^2}C_{HW} + \frac{1}{g_Y^2}C_{HB} - \frac{1}{g_L g_Y}C_{HWB}\right), \\
c_{zz} &= 4\left(\frac{g_L^2 C_{HW} + g_Y^2 C_{HB} + g_L g_Y C_{HWB}}{(g_L^2 + g_Y^2)^2}\right), \\
c_{z\gamma} &= 4\left(\frac{C_{HW} - C_{HB} - \frac{g_L^2 - g_Y^2}{2g_L g_Y}C_{HWB}}{g_L^2 + g_Y^2}\right),
\end{aligned}
\tag{A.40}
$$

where

$$
f(T^3, Q) \equiv \left\{-Q\frac{g_L g_Y}{g_L^2 - g_Y^2}C_{HWB} - \mathbf{1}\left(\frac{1}{4}C_{HD} + \frac{1}{2}\Delta_{G_F}\right)\left(T^3 + Q\frac{g_Y^2}{g_L^2 - g_Y^2}\right)\right\}\mathbf{1}, \tag{A.41}
$$

and $\Delta_{G_F} = [C_{Hl}^{(3)}]_{11} + [C_{Hl}^{(3)}]_{22} - \frac{1}{2}[C_{ll}]_{1221}$. To these coefficients, the fit in ref. [121] also adds those for the dimension-6 Yukawa-like operators of top, bottom, muon and tau fermions, as well as the one responsible for modifying the muon decay: $[C_{uH}]_{33}$, $[C_{dH}]_{33}$, $[C_{eH}]_{22}$, $[C_{eH}]_{33}$, $[C_{ll}]_{1221}$.

The set of $\delta g_{V\psi}$ parametrise the corresponding vertex corrections of Z and W bosons, and are mostly constrained by electroweak data from LEP. As mentioned, the coefficient $[C_{ll}]_{1221}$ enters the EW fit by its impact in the muon decay. Finally, the other coefficients do not affect EW observables at tree level and are only constrained by Higgs data.

Class	Coefficients	Warsaw basis	95% CL Individual	95% CL Marginalised
Dipoles	c_{tG}	C_{uG}	[0.01,0.11]	[0.01,0.23]
	c_{tW}	C_{uW}	[-0.085,0.030]	[-0.28,0.13]
	c_{tZ}	$-s_\theta\, C_{uB} + c_\theta\, C_{uW}$	[-0.038,0.090]	[-0.50,0.14]
Higgs-Top	c_{HQ}^3	$C_{Hq}^{(3)}$	[-0.39,0.34]	[-0.42,0.31]
	$c_{HQ}^{(-)}$	$C_{Hq}^{(1)} - C_{Hq}^{(3)}$	[-1.1,1.5]	[-2.7,2.7]
	c_{Ht}	C_{Hu}	[-2.8,2.2]	[-15,4]
	c_{tH}	C_{uH}	[-1.3,0.4]	[-0.5,2.9]
4 quarks	c_{QQ}^1	$2C_{qq}^{(1)} - \frac{2}{3}C_{qq}^{(3)}$	[-2.3,2.0]	[-3.7,4.4]
	c_{QQ}^8	$8C_{qq}^{(3)}$	[-6.8,5.9]	[-13,10]
	c_{Qt}^1	$C_{qu}^{(1)}$	[-1.8,1.9]	[-1.5,1.4]
	c_{Qt}^8	$C_{qu}^{(8)}$	[-4.3,3.3]	[-3.4,2.5]
	c_{tt}^1	C_{uu}	[-1.1,1.0]	[-0.88,0.81]

Table 14. The 95% CL bounds from SMEFiT for individual and global fits obtained using quadratic EFT calculations. Top quark, Higgs and diboson data have been used, as discussed in ref. [130]. Coefficients are expressed in both the SMEFiT and the Warsaw basis conventions.

A.10 Direct constraints from LHC

Here we provide the 95% CL bounds on Wilson coefficients, from both individual and global marginalised fits obtained from SMEFiT [130]. These are illustrated in table 14. Single parameter fits match the findings of ref. [130] (see table 5.4 therein).

Even though it is reasonable to expect that individual bounds are comparable or more severe than the global ones, we observe the latter to be stronger in the case of the $C_{qu}^{(1/8)}$ and C_{uu} coefficients. This surprising trend was also observed in ref. [130], where the global analysis involved a larger set of operators.

The direct bounds shown in table 14 are compared to the indirect limits computed in this work in section 4.

$\nu\nu$ + h.c.	
$\mathcal{O}_\nu$	$(\nu_{Lp}^T C \nu_{Lr})$

$(\nu\nu)X$ + h.c.	
$\mathcal{O}_{\nu\gamma}$	$(\nu_{Lp}^T C \sigma^{\mu\nu}\nu_{Lr})F_{\mu\nu}$

$(\overline{L}R)X$ + h.c.	
$\mathcal{O}_{e\gamma}$	$\bar{e}_{Lp}\sigma^{\mu\nu}e_{Rr}\,F_{\mu\nu}$
$\mathcal{O}_{u\gamma}$	$\bar{u}_{Lp}\sigma^{\mu\nu}u_{Rr}\,F_{\mu\nu}$
$\mathcal{O}_{d\gamma}$	$\bar{d}_{Lp}\sigma^{\mu\nu}d_{Rr}\,F_{\mu\nu}$
$\mathcal{O}_{uG}$	$\bar{u}_{Lp}\sigma^{\mu\nu}T^A u_{Rr}\,G^A_{\mu\nu}$
$\mathcal{O}_{dG}$	$\bar{d}_{Lp}\sigma^{\mu\nu}T^A d_{Rr}\,G^A_{\mu\nu}$

X^3	
$\mathcal{O}_G$	$f^{ABC}G^{A\nu}_\mu G^{B\rho}_\nu G^{C\mu}_\rho$
$\mathcal{O}_{\widetilde{G}}$	$f^{ABC}\widetilde{G}^{A\nu}_\mu G^{B\rho}_\nu G^{C\mu}_\rho$

$(\overline{L}L)(\overline{L}L)$	
$\mathcal{O}^{V,LL}_{\nu\nu}$	$(\bar{\nu}_{Lp}\gamma^\mu\nu_{Lr})(\bar{\nu}_{Ls}\gamma_\mu\nu_{Lt})$
$\mathcal{O}^{V,LL}_{ee}$	$(\bar{e}_{Lp}\gamma^\mu e_{Lr})(\bar{e}_{Ls}\gamma_\mu e_{Lt})$
$\mathcal{O}^{V,LL}_{\nu e}$	$(\bar{\nu}_{Lp}\gamma^\mu\nu_{Lr})(\bar{e}_{Ls}\gamma_\mu e_{Lt})$
$\mathcal{O}^{V,LL}_{\nu u}$	$(\bar{\nu}_{Lp}\gamma^\mu\nu_{Lr})(\bar{u}_{Ls}\gamma_\mu u_{Lt})$
$\mathcal{O}^{V,LL}_{\nu d}$	$(\bar{\nu}_{Lp}\gamma^\mu\nu_{Lr})(\bar{d}_{Ls}\gamma_\mu d_{Lt})$
$\mathcal{O}^{V,LL}_{eu}$	$(\bar{e}_{Lp}\gamma^\mu e_{Lr})(\bar{u}_{Ls}\gamma_\mu u_{Lt})$
$\mathcal{O}^{V,LL}_{ed}$	$(\bar{e}_{Lp}\gamma^\mu e_{Lr})(\bar{d}_{Ls}\gamma_\mu d_{Lt})$
$\mathcal{O}^{V,LL}_{\nu edu}$	$(\bar{\nu}_{Lp}\gamma^\mu e_{Lr})(\bar{d}_{Ls}\gamma_\mu u_{Lt})$ + h.c.
$\mathcal{O}^{V,LL}_{uu}$	$(\bar{u}_{Lp}\gamma^\mu u_{Lr})(\bar{u}_{Ls}\gamma_\mu u_{Lt})$
$\mathcal{O}^{V,LL}_{dd}$	$(\bar{d}_{Lp}\gamma^\mu d_{Lr})(\bar{d}_{Ls}\gamma_\mu d_{Lt})$
$\mathcal{O}^{V1,LL}_{ud}$	$(\bar{u}_{Lp}\gamma^\mu u_{Lr})(\bar{d}_{Ls}\gamma_\mu d_{Lt})$
$\mathcal{O}^{V8,LL}_{ud}$	$(\bar{u}_{Lp}\gamma^\mu T^A u_{Lr})(\bar{d}_{Ls}\gamma_\mu T^A d_{Lt})$

$(\overline{R}R)(\overline{R}R)$	
$\mathcal{O}^{V,RR}_{ee}$	$(\bar{e}_{Rp}\gamma^\mu e_{Rr})(\bar{e}_{Rs}\gamma_\mu e_{Rt})$
$\mathcal{O}^{V,RR}_{eu}$	$(\bar{e}_{Rp}\gamma^\mu e_{Rr})(\bar{u}_{Rs}\gamma_\mu u_{Rt})$
$\mathcal{O}^{V,RR}_{ed}$	$(\bar{e}_{Rp}\gamma^\mu e_{Rr})(\bar{d}_{Rs}\gamma_\mu d_{Rt})$
$\mathcal{O}^{V,RR}_{uu}$	$(\bar{u}_{Rp}\gamma^\mu u_{Rr})(\bar{u}_{Rs}\gamma_\mu u_{Rt})$
$\mathcal{O}^{V,RR}_{dd}$	$(\bar{d}_{Rp}\gamma^\mu d_{Rr})(\bar{d}_{Rs}\gamma_\mu d_{Rt})$
$\mathcal{O}^{V1,RR}_{ud}$	$(\bar{u}_{Rp}\gamma^\mu u_{Rr})(\bar{d}_{Rs}\gamma_\mu d_{Rt})$
$\mathcal{O}^{V8,RR}_{ud}$	$(\bar{u}_{Rp}\gamma^\mu T^A u_{Rr})(\bar{d}_{Rs}\gamma_\mu T^A d_{Rt})$

$(\overline{L}L)(\overline{R}R)$	
$\mathcal{O}^{V,LR}_{\nu e}$	$(\bar{\nu}_{Lp}\gamma^\mu\nu_{Lr})(\bar{e}_{Rs}\gamma_\mu e_{Rt})$
$\mathcal{O}^{V,LR}_{ee}$	$(\bar{e}_{Lp}\gamma^\mu e_{Lr})(\bar{e}_{Rs}\gamma_\mu e_{Rt})$
$\mathcal{O}^{V,LR}_{\nu u}$	$(\bar{\nu}_{Lp}\gamma^\mu\nu_{Lr})(\bar{u}_{Rs}\gamma_\mu u_{Rt})$
$\mathcal{O}^{V,LR}_{\nu d}$	$(\bar{\nu}_{Lp}\gamma^\mu\nu_{Lr})(\bar{d}_{Rs}\gamma_\mu d_{Rt})$
$\mathcal{O}^{V,LR}_{eu}$	$(\bar{e}_{Lp}\gamma^\mu e_{Lr})(\bar{u}_{Rs}\gamma_\mu u_{Rt})$
$\mathcal{O}^{V,LR}_{ed}$	$(\bar{e}_{Lp}\gamma^\mu e_{Lr})(\bar{d}_{Rs}\gamma_\mu d_{Rt})$
$\mathcal{O}^{V,LR}_{ue}$	$(\bar{u}_{Lp}\gamma^\mu u_{Lr})(\bar{e}_{Rs}\gamma_\mu e_{Rt})$
$\mathcal{O}^{V,LR}_{de}$	$(\bar{d}_{Lp}\gamma^\mu d_{Lr})(\bar{e}_{Rs}\gamma_\mu e_{Rt})$
$\mathcal{O}^{V,LR}_{\nu edu}$	$(\bar{\nu}_{Lp}\gamma^\mu e_{Lr})(\bar{d}_{Rs}\gamma_\mu u_{Rt})$ + h.c.
$\mathcal{O}^{V1,LR}_{uu}$	$(\bar{u}_{Lp}\gamma^\mu u_{Lr})(\bar{u}_{Rs}\gamma_\mu u_{Rt})$
$\mathcal{O}^{V8,LR}_{uu}$	$(\bar{u}_{Lp}\gamma^\mu T^A u_{Lr})(\bar{u}_{Rs}\gamma_\mu T^A u_{Rt})$
$\mathcal{O}^{V1,LR}_{ud}$	$(\bar{u}_{Lp}\gamma^\mu u_{Lr})(\bar{d}_{Rs}\gamma_\mu d_{Rt})$
$\mathcal{O}^{V8,LR}_{ud}$	$(\bar{u}_{Lp}\gamma^\mu T^A u_{Lr})(\bar{d}_{Rs}\gamma_\mu T^A d_{Rt})$
$\mathcal{O}^{V1,LR}_{du}$	$(\bar{d}_{Lp}\gamma^\mu d_{Lr})(\bar{u}_{Rs}\gamma_\mu u_{Rt})$
$\mathcal{O}^{V8,LR}_{du}$	$(\bar{d}_{Lp}\gamma^\mu T^A d_{Lr})(\bar{u}_{Rs}\gamma_\mu T^A u_{Rt})$
$\mathcal{O}^{V1,LR}_{dd}$	$(\bar{d}_{Lp}\gamma^\mu d_{Lr})(\bar{d}_{Rs}\gamma_\mu d_{Rt})$
$\mathcal{O}^{V8,LR}_{dd}$	$(\bar{d}_{Lp}\gamma^\mu T^A d_{Lr})(\bar{d}_{Rs}\gamma_\mu T^A d_{Rt})$
$\mathcal{O}^{V1,LR}_{uddu}$	$(\bar{u}_{Lp}\gamma^\mu d_{Lr})(\bar{d}_{Rs}\gamma_\mu u_{Rt})$ + h.c.
$\mathcal{O}^{V8,LR}_{uddu}$	$(\bar{u}_{Lp}\gamma^\mu T^A d_{Lr})(\bar{d}_{Rs}\gamma_\mu T^A u_{Rt})$ + h.c.

$(\overline{L}R)(\overline{L}R)$ + h.c.	
$\mathcal{O}^{S,RR}_{ee}$	$(\bar{e}_{Lp}e_{Rr})(\bar{e}_{Ls}e_{Rt})$
$\mathcal{O}^{S,RR}_{eu}$	$(\bar{e}_{Lp}e_{Rr})(\bar{u}_{Ls}u_{Rt})$
$\mathcal{O}^{T,RR}_{eu}$	$(\bar{e}_{Lp}\sigma^{\mu\nu}e_{Rr})(\bar{u}_{Ls}\sigma_{\mu\nu}u_{Rt})$
$\mathcal{O}^{S,RR}_{ed}$	$(\bar{e}_{Lp}e_{Rr})(\bar{d}_{Ls}d_{Rt})$
$\mathcal{O}^{T,RR}_{ed}$	$(\bar{e}_{Lp}\sigma^{\mu\nu}e_{Rr})(\bar{d}_{Ls}\sigma_{\mu\nu}d_{Rt})$
$\mathcal{O}^{S,RR}_{\nu edu}$	$(\bar{\nu}_{Lp}e_{Rr})(\bar{d}_{Ls}u_{Rt})$
$\mathcal{O}^{T,RR}_{\nu edu}$	$(\bar{\nu}_{Lp}\sigma^{\mu\nu}e_{Rr})(\bar{d}_{Ls}\sigma_{\mu\nu}u_{Rt})$
$\mathcal{O}^{S1,RR}_{uu}$	$(\bar{u}_{Lp}u_{Rr})(\bar{u}_{Ls}u_{Rt})$
$\mathcal{O}^{S8,RR}_{uu}$	$(\bar{u}_{Lp}T^A u_{Rr})(\bar{u}_{Ls}T^A u_{Rt})$
$\mathcal{O}^{S1,RR}_{ud}$	$(\bar{u}_{Lp}u_{Rr})(\bar{d}_{Ls}d_{Rt})$
$\mathcal{O}^{S8,RR}_{ud}$	$(\bar{u}_{Lp}T^A u_{Rr})(\bar{d}_{Ls}T^A d_{Rt})$
$\mathcal{O}^{S1,RR}_{dd}$	$(\bar{d}_{Lp}d_{Rr})(\bar{d}_{Ls}d_{Rt})$
$\mathcal{O}^{S8,RR}_{dd}$	$(\bar{d}_{Lp}T^A d_{Rr})(\bar{d}_{Ls}T^A d_{Rt})$
$\mathcal{O}^{S1,RR}_{uddu}$	$(\bar{u}_{Lp}d_{Rr})(\bar{d}_{Ls}u_{Rt})$
$\mathcal{O}^{S8,RR}_{uddu}$	$(\bar{u}_{Lp}T^A d_{Rr})(\bar{d}_{Ls}T^A u_{Rt})$

$(\overline{L}R)(\overline{R}L)$ + h.c.	
$\mathcal{O}^{S,RL}_{eu}$	$(\bar{e}_{Lp}e_{Rr})(\bar{u}_{Rs}u_{Lt})$
$\mathcal{O}^{S,RL}_{ed}$	$(\bar{e}_{Lp}e_{Rr})(\bar{d}_{Rs}d_{Lt})$
$\mathcal{O}^{S,RL}_{\nu edu}$	$(\bar{\nu}_{Lp}e_{Rr})(\bar{d}_{Rs}u_{Lt})$

Table 15. LEFT operators of dimension three and five, as well as LEFT operators of dimension six that conserve baryon and lepton number, reproduced from ref. [16].

References

[1] S.L. Glashow, J. Iliopoulos and L. Maiani, *Weak Interactions with Lepton-Hadron Symmetry*, *Phys. Rev. D* **2** (1970) 1285 [INSPIRE].

[2] R. Franceschini, *Beyond-Standard-Model Physics Associated with the Top Quark*, arXiv:2301.04407 [INSPIRE].

[3] B. Grzadkowski, M. Iskrzynski, M. Misiak and J. Rosiek, *Dimension-Six Terms in the Standard Model Lagrangian*, *JHEP* **10** (2010) 085 [arXiv:1008.4884] [INSPIRE].

[4] R. Barbieri et al., U(2) *and Minimal Flavour Violation in Supersymmetry*, *Eur. Phys. J. C* **71** (2011) 1725 [arXiv:1105.2296] [INSPIRE].

[5] R. Barbieri, D. Buttazzo, F. Sala and D.M. Straub, *Flavour physics from an approximate* U(2)^3 *symmetry*, *JHEP* **07** (2012) 181 [arXiv:1203.4218] [INSPIRE].

[6] R. Barbieri et al., *A 125 GeV composite Higgs boson versus flavour and electroweak precision tests*, *JHEP* **05** (2013) 069 [arXiv:1211.5085] [INSPIRE].

[7] D.A. Faroughy, G. Isidori, F. Wilsch and K. Yamamoto, *Flavour symmetries in the SMEFT*, *JHEP* **08** (2020) 166 [arXiv:2005.05366] [INSPIRE].

[8] P.J. Fox et al., *Deciphering top flavor violation at the LHC with B factories*, *Phys. Rev. D* **78** (2008) 054008 [arXiv:0704.1482] [INSPIRE].

[9] B. Grzadkowski and M. Misiak, *Anomalous Wtb coupling effects in the weak radiative B-meson decay*, *Phys. Rev. D* **78** (2008) 077501 [*Erratum ibid.* **84** (2011) 059903] [arXiv:0802.1413] [INSPIRE].

[10] J. Drobnak, S. Fajfer and J.F. Kamenik, *Probing anomalous tWb interactions with rare B decays*, *Nucl. Phys. B* **855** (2012) 82 [arXiv:1109.2357] [INSPIRE].

[11] J. Brod, A. Greljo, E. Stamou and P. Uttayarat, *Probing anomalous $t\bar{t}Z$ interactions with rare meson decays*, *JHEP* **02** (2015) 141 [arXiv:1408.0792] [INSPIRE].

[12] W. Altmannshofer, S. Gori, B.V. Lehmann and J. Zuo, *UV physics from IR features: new prospects from top flavor violation*, *Phys. Rev. D* **107** (2023) 095025 [arXiv:2303.00781] [INSPIRE].

[13] V. Cirigliano, W. Dekens, J. de Vries and E. Mereghetti, *Constraining the top-Higgs sector of the Standard Model Effective Field Theory*, *Phys. Rev. D* **94** (2016) 034031 [arXiv:1605.04311] [INSPIRE].

[14] S. Bißmann et al., *Constraining top-quark couplings combining top-quark and $\bm{B}$ decay observables*, *Eur. Phys. J. C* **80** (2020) 136 [arXiv:1909.13632] [INSPIRE].

[15] S. Bißmann, C. Grunwald, G. Hiller and K. Kröninger, *Top and Beauty synergies in SMEFT-fits at present and future colliders*, *JHEP* **06** (2021) 010 [arXiv:2012.10456] [INSPIRE].

[16] E.E. Jenkins, A.V. Manohar and P. Stoffer, *Low-Energy Effective Field Theory below the Electroweak Scale: Operators and Matching*, *JHEP* **03** (2018) 016 [arXiv:1709.04486] [INSPIRE].

[17] A. Celis, J. Fuentes-Martín, A. Vicente and J. Virto, *DsixTools: the Standard Model Effective Field Theory Toolkit*, *Eur. Phys. J. C* **77** (2017) 405 [arXiv:1704.04504] [INSPIRE].

[18] J. Fuentes-Martin, P. Ruiz-Femenia, A. Vicente and J. Virto, *DsixTools 2.0: the Effective Field Theory Toolkit*, *Eur. Phys. J. C* **81** (2021) 167 [arXiv:2010.16341] [INSPIRE].

[19] E.E. Jenkins, A.V. Manohar and M. Trott, *Renormalization Group Evolution of the Standard Model Dimension Six Operators I: formalism and lambda Dependence*, *JHEP* **10** (2013) 087 [arXiv:1308.2627] [INSPIRE].

[20] E.E. Jenkins, A.V. Manohar and M. Trott, *Renormalization Group Evolution of the Standard Model Dimension Six Operators II: Yukawa Dependence*, *JHEP* **01** (2014) 035 [arXiv:1310.4838] [INSPIRE].

[21] R. Alonso, E.E. Jenkins, A.V. Manohar and M. Trott, *Renormalization Group Evolution of the Standard Model Dimension Six Operators III: Gauge Coupling Dependence and Phenomenology*, *JHEP* **04** (2014) 159 [arXiv:1312.2014] [INSPIRE].

[22] J. Braathen et al., *N-loop running should be combined with N-loop matching*, *Phys. Rev. D* **97** (2018) 015011 [arXiv:1711.08460] [INSPIRE].

[23] W. Dekens and P. Stoffer, *Low-energy effective field theory below the electroweak scale: matching at one loop*, *JHEP* **10** (2019) 197 [*Erratum ibid.* **11** (2022) 148] [arXiv:1908.05295] [INSPIRE].

[24] J. Aebischer, A. Crivellin, M. Fael and C. Greub, *Matching of gauge invariant dimension-six operators for $b \to s$ and $b \to c$ transitions*, *JHEP* **05** (2016) 037 [arXiv:1512.02830] [INSPIRE].

[25] E.E. Jenkins, A.V. Manohar and P. Stoffer, *Low-Energy Effective Field Theory below the Electroweak Scale: Anomalous Dimensions*, *JHEP* **01** (2018) 084 [arXiv:1711.05270] [INSPIRE].

[26] T. van Ritbergen, J.A.M. Vermaseren and S.A. Larin, *The Four loop beta function in quantum chromodynamics*, *Phys. Lett. B* **400** (1997) 379 [hep-ph/9701390] [INSPIRE].

[27] J.A.M. Vermaseren, S.A. Larin and T. van Ritbergen, *The four loop quark mass anomalous dimension and the invariant quark mass*, *Phys. Lett. B* **405** (1997) 327 [hep-ph/9703284] [INSPIRE].

[28] P.A. Baikov, K.G. Chetyrkin and J.H. Kühn, *Five-loop fermion anomalous dimension for a general gauge group from four-loop massless propagators*, *JHEP* **04** (2017) 119 [arXiv:1702.01458] [INSPIRE].

[29] K.G. Chetyrkin, J.H. Kuhn and M. Steinhauser, *RunDec: a mathematica package for running and decoupling of the strong coupling and quark masses*, *Comput. Phys. Commun.* **133** (2000) 43 [hep-ph/0004189] [INSPIRE].

[30] A.V. Bednyakov, A.F. Pikelner and V.N. Velizhanin, *Anomalous dimensions of gauge fields and gauge coupling beta-functions in the Standard Model at three loops*, *JHEP* **01** (2013) 017 [arXiv:1210.6873] [INSPIRE].

[31] A.V. Bednyakov, A.F. Pikelner and V.N. Velizhanin, *Yukawa coupling beta-functions in the Standard Model at three loops*, *Phys. Lett. B* **722** (2013) 336 [arXiv:1212.6829] [INSPIRE].

[32] A.V. Bednyakov, A.F. Pikelner and V.N. Velizhanin, *Higgs self-coupling beta-function in the Standard Model at three loops*, *Nucl. Phys. B* **875** (2013) 552 [arXiv:1303.4364] [INSPIRE].

[33] A.V. Bednyakov, A.F. Pikelner and V.N. Velizhanin, *Three-loop SM beta-functions for matrix Yukawa couplings*, *Phys. Lett. B* **737** (2014) 129 [arXiv:1406.7171] [INSPIRE].

[34] LHCb collaboration, *Test of lepton universality in $b \to s\ell^+\ell^-$ decays, Phys. Rev. Lett.* **131** (2023) 051803 [arXiv:2212.09152] [INSPIRE].

[35] D. Bečirević, G. Piazza and O. Sumensari, *Revisiting $B \to K^{(*)}\nu\bar{\nu}$ decays in the Standard Model and beyond, Eur. Phys. J. C* **83** (2023) 252 [arXiv:2301.06990] [INSPIRE].

[36] E. Ganiev, *Recent Belle II results on radiative and electroweak penguin decays*, in proceedings of *EPS-HEP2023 conference*, Universität Hamburg, 24th August 2023, https://indico.desy.de/event/34916/contributions/146877/.

[37] BELLE collaboration, *Search for $B \to h\nu\bar{\nu}$ decays with semileptonic tagging at Belle, Phys. Rev. D* **96** (2017) 091101 [*Addendum ibid.* **97** (2018) 099902] [arXiv:1702.03224] [INSPIRE].

[38] PARTICLE DATA GROUP collaboration, *Review of Particle Physics, PTEP* **2022** (2022) 083C01 [INSPIRE].

[39] BELLE collaboration, *Test of lepton flavor universality and search for lepton flavor violation in $B \to K\ell\ell$ decays, JHEP* **03** (2021) 105 [arXiv:1908.01848] [INSPIRE].

[40] BaBar collaboration, *A search for the decay modes $B^{+-} \to h^{+-}\tau^{+-}l$, Phys. Rev. D* **86** (2012) 012004 [arXiv:1204.2852] [INSPIRE].

[41] LHCb collaboration, *Search for the lepton flavour violating decay $B^+ \to K^+\mu^-\tau^+$ using B^{*0}_{s2} decays, JHEP* **06** (2020) 129 [arXiv:2003.04352] [INSPIRE].

[42] LHCb collaboration, *Search for the Rare Decays $B^0_s \to e^+e^-$ and $B^0 \to e^+e^-$, Phys. Rev. Lett.* **124** (2020) 211802 [arXiv:2003.03999] [INSPIRE].

[43] LHCb collaboration, *Measurement of the $B^0_s \to \mu^+\mu^-$ decay properties and search for the $B^0 \to \mu^+\mu^-$ and $B^0_s \to \mu^+\mu^-\gamma$ decays, Phys. Rev. D* **105** (2022) 012010 [arXiv:2108.09283] [INSPIRE].

[44] LHCb collaboration, *Search for the decays $B^0_s \to \tau^+\tau^-$ and $B^0 \to \tau^+\tau^-$, Phys. Rev. Lett.* **118** (2017) 251802 [arXiv:1703.02508] [INSPIRE].

[45] LHCb collaboration, *Search for the lepton-flavour violating decays $B^0_{(s)} \to e^\pm\mu^\mp$, JHEP* **03** (2018) 078 [arXiv:1710.04111] [INSPIRE].

[46] LHCb collaboration, *Search for the lepton-flavour-violating decays $B^0_s \to \tau^\pm\mu^\mp$ and $B^0 \to \tau^\pm\mu^\mp$, Phys. Rev. Lett.* **123** (2019) 211801 [arXiv:1905.06614] [INSPIRE].

[47] NA62 collaboration, *Measurement of the very rare $K^+ \to \pi^+\nu\bar{\nu}$ decay, JHEP* **06** (2021) 093 [arXiv:2103.15389] [INSPIRE].

[48] E949 collaboration, *New measurement of the $K^+ \to \pi^+\nu\bar{\nu}$ branching ratio, Phys. Rev. Lett.* **101** (2008) 191802 [arXiv:0808.2459] [INSPIRE].

[49] KOTO collaboration, *Search for the $K_L \to \pi^0\nu\bar{\nu}$ and $K_L \to \pi^0 X^0$ decays at the J-PARC KOTO experiment, Phys. Rev. Lett.* **122** (2019) 021802 [arXiv:1810.09655] [INSPIRE].

[50] LHCb collaboration, *Constraints on the $K^0_S \to \mu^+\mu^-$ Branching Fraction, Phys. Rev. Lett.* **125** (2020) 231801 [arXiv:2001.10354] [INSPIRE].

[51] G. Isidori and R. Unterdorfer, *On the short distance constraints from $K(L,S) \to \mu^+\mu^-$, JHEP* **01** (2004) 009 [hep-ph/0311084] [INSPIRE].

[52] BNL collaboration, *New limit on muon and electron lepton number violation from $K0(L) \to \mu^\pm e^{-+}$ decay, Phys. Rev. Lett.* **81** (1998) 5734 [hep-ex/9811038] [INSPIRE].

[53] KTEV collaboration, *Search for the Decay* $K_L \to \pi^0 \mu^+ \mu^-$, *Phys. Rev. Lett.* **84** (2000) 5279 [hep-ex/0001006] [INSPIRE].

[54] KTEV collaboration, *Search for the rare decay* $K(L) \to pi0 \, e^+e^-$, *Phys. Rev. Lett.* **93** (2004) 021805 [hep-ex/0309072] [INSPIRE].

[55] KTEV collaboration, *Search for lepton flavor violating decays of the neutral kaon*, *Phys. Rev. Lett.* **100** (2008) 131803 [arXiv:0711.3472] [INSPIRE].

[56] NA62 collaboration, *Search for Lepton Number and Flavor Violation in* K^+ *and* π^0 *Decays*, *Phys. Rev. Lett.* **127** (2021) 131802 [arXiv:2105.06759] [INSPIRE].

[57] A.J. Buras and E. Venturini, *The exclusive vision of rare K and B decays and of the quark mixing in the standard model*, *Eur. Phys. J. C* **82** (2022) 615 [arXiv:2203.11960] [INSPIRE].

[58] J. Aebischer, C. Bobeth, A.J. Buras and J. Kumar, *SMEFT ATLAS of* $\Delta F = 2$ *transitions*, *JHEP* **12** (2020) 187 [arXiv:2009.07276] [INSPIRE].

[59] V. Cirigliano et al., *Semileptonic tau decays beyond the Standard Model*, *JHEP* **04** (2022) 152 [arXiv:2112.02087] [INSPIRE].

[60] M. González-Alonso and J. Martin Camalich, *Global Effective-Field-Theory analysis of New-Physics effects in (semi)leptonic kaon decays*, *JHEP* **12** (2016) 052 [arXiv:1605.07114] [INSPIRE].

[61] A. Falkowski, M. González-Alonso and O. Naviliat-Cuncic, *Comprehensive analysis of beta decays within and beyond the Standard Model*, *JHEP* **04** (2021) 126 [arXiv:2010.13797] [INSPIRE].

[62] HFLAV collaboration, *Averages of b-hadron, c-hadron, and* τ*-lepton properties as of 2021*, *Phys. Rev. D* **107** (2023) 052008 [arXiv:2206.07501] [INSPIRE].

[63] J. Aebischer et al., *Effective field theory interpretation of lepton magnetic and electric dipole moments*, *JHEP* **07** (2021) 107 [arXiv:2102.08954] [INSPIRE].

[64] L. Morel, Z. Yao, P. Cladé and S. Guellati-Khélifa, *Determination of the fine-structure constant with an accuracy of 81 parts per trillion*, *Nature* **588** (2020) 61 [INSPIRE].

[65] R.H. Parker et al., *Measurement of the fine-structure constant as a test of the Standard Model*, *Science* **360** (2018) 191 [arXiv:1812.04130] [INSPIRE].

[66] T. Aoyama et al., *The anomalous magnetic moment of the muon in the Standard Model*, *Phys. Rept.* **887** (2020) 1 [arXiv:2006.04822] [INSPIRE].

[67] T. Aoyama, M. Hayakawa, T. Kinoshita and M. Nio, *Complete Tenth-Order QED Contribution to the Muon g-2*, *Phys. Rev. Lett.* **109** (2012) 111808 [arXiv:1205.5370] [INSPIRE].

[68] T. Aoyama, T. Kinoshita and M. Nio, *Theory of the Anomalous Magnetic Moment of the Electron*, *Atoms* **7** (2019) 28 [INSPIRE].

[69] A. Czarnecki, W.J. Marciano and A. Vainshtein, *Refinements in electroweak contributions to the muon anomalous magnetic moment*, *Phys. Rev. D* **67** (2003) 073006 [*Erratum ibid.* **73** (2006) 119901] [hep-ph/0212229] [INSPIRE].

[70] C. Gnendiger, D. Stöckinger and H. Stöckinger-Kim, *The electroweak contributions to* $(g-2)_\mu$ *after the Higgs boson mass measurement*, *Phys. Rev. D* **88** (2013) 053005 [arXiv:1306.5546] [INSPIRE].

[71] M. Davier, A. Hoecker, B. Malaescu and Z. Zhang, *Reevaluation of the hadronic vacuum polarisation contributions to the Standard Model predictions of the muon $g - 2$ and $\alpha(m_Z^2)$ using newest hadronic cross-section data*, *Eur. Phys. J. C* **77** (2017) 827 [arXiv:1706.09436] [INSPIRE].

[72] A. Keshavarzi, D. Nomura and T. Teubner, *Muon $g - 2$ and $\alpha(M_Z^2)$: a new data-based analysis*, *Phys. Rev. D* **97** (2018) 114025 [arXiv:1802.02995] [INSPIRE].

[73] G. Colangelo, M. Hoferichter and P. Stoffer, *Two-pion contribution to hadronic vacuum polarization*, *JHEP* **02** (2019) 006 [arXiv:1810.00007] [INSPIRE].

[74] M. Hoferichter, B.-L. Hoid and B. Kubis, *Three-pion contribution to hadronic vacuum polarization*, *JHEP* **08** (2019) 137 [arXiv:1907.01556] [INSPIRE].

[75] M. Davier, A. Hoecker, B. Malaescu and Z. Zhang, *A new evaluation of the hadronic vacuum polarisation contributions to the muon anomalous magnetic moment and to* $\boldsymbol{\alpha(\mathrm{m_Z^2})}$, *Eur. Phys. J. C* **80** (2020) 241 [*Erratum ibid.* **80** (2020) 410] [arXiv:1908.00921] [INSPIRE].

[76] A. Keshavarzi, D. Nomura and T. Teubner, *$g - 2$ of charged leptons, $\alpha(M_Z^2)$, and the hyperfine splitting of muonium*, *Phys. Rev. D* **101** (2020) 014029 [arXiv:1911.00367] [INSPIRE].

[77] A. Kurz, T. Liu, P. Marquard and M. Steinhauser, *Hadronic contribution to the muon anomalous magnetic moment to next-to-next-to-leading order*, *Phys. Lett. B* **734** (2014) 144 [arXiv:1403.6400] [INSPIRE].

[78] K. Melnikov and A. Vainshtein, *Hadronic light-by-light scattering contribution to the muon anomalous magnetic moment revisited*, *Phys. Rev. D* **70** (2004) 113006 [hep-ph/0312226] [INSPIRE].

[79] P. Masjuan and P. Sanchez-Puertas, *Pseudoscalar-pole contribution to the $(g_\mu - 2)$: a rational approach*, *Phys. Rev. D* **95** (2017) 054026 [arXiv:1701.05829] [INSPIRE].

[80] G. Colangelo, M. Hoferichter, M. Procura and P. Stoffer, *Dispersion relation for hadronic light-by-light scattering: two-pion contributions*, *JHEP* **04** (2017) 161 [arXiv:1702.07347] [INSPIRE].

[81] M. Hoferichter et al., *Dispersion relation for hadronic light-by-light scattering: pion pole*, *JHEP* **10** (2018) 141 [arXiv:1808.04823] [INSPIRE].

[82] A. Gérardin, H.B. Meyer and A. Nyffeler, *Lattice calculation of the pion transition form factor with $N_f = 2 + 1$ Wilson quarks*, *Phys. Rev. D* **100** (2019) 034520 [arXiv:1903.09471] [INSPIRE].

[83] J. Bijnens, N. Hermansson-Truedsson and A. Rodríguez-Sánchez, *Short-distance constraints for the HLbL contribution to the muon anomalous magnetic moment*, *Phys. Lett. B* **798** (2019) 134994 [arXiv:1908.03331] [INSPIRE].

[84] G. Colangelo et al., *Longitudinal short-distance constraints for the hadronic light-by-light contribution to $(g - 2)_\mu$ with large-N_c Regge models*, *JHEP* **03** (2020) 101 [arXiv:1910.13432] [INSPIRE].

[85] T. Blum et al., *Hadronic Light-by-Light Scattering Contribution to the Muon Anomalous Magnetic Moment from Lattice QCD*, *Phys. Rev. Lett.* **124** (2020) 132002 [arXiv:1911.08123] [INSPIRE].

[86] G. Colangelo et al., *Remarks on higher-order hadronic corrections to the muon g−2*, *Phys. Lett. B* **735** (2014) 90 [arXiv:1403.7512] [INSPIRE].

[87] S. Borsanyi et al., *Leading hadronic contribution to the muon magnetic moment from lattice QCD*, *Nature* **593** (2021) 51 [arXiv:2002.12347] [INSPIRE].

[88] C. Lehner and A.S. Meyer, *Consistency of hadronic vacuum polarization between lattice QCD and the R-ratio*, *Phys. Rev. D* **101** (2020) 074515 [arXiv:2003.04177] [INSPIRE].

[89] M. Cè et al., *The hadronic running of the electromagnetic coupling and the electroweak mixing angle from lattice QCD*, *JHEP* **08** (2022) 220 [arXiv:2203.08676] [INSPIRE].

[90] M. Cè et al., *Window observable for the hadronic vacuum polarization contribution to the muon g-2 from lattice QCD*, *Phys. Rev. D* **106** (2022) 114502 [arXiv:2206.06582] [INSPIRE].

[91] CHIQCD collaboration, *Muon g-2 with overlap valence fermions*, *Phys. Rev. D* **107** (2023) 034513 [arXiv:2204.01280] [INSPIRE].

[92] EXTENDED TWISTED MASS collaboration, *Lattice calculation of the short and intermediate time-distance hadronic vacuum polarization contributions to the muon magnetic moment using twisted-mass fermions*, *Phys. Rev. D* **107** (2023) 074506 [arXiv:2206.15084] [INSPIRE].

[93] G. Colangelo et al., *Data-driven evaluations of Euclidean windows to scrutinize hadronic vacuum polarization*, *Phys. Lett. B* **833** (2022) 137313 [arXiv:2205.12963] [INSPIRE].

[94] C. Aubin, T. Blum, M. Golterman and S. Peris, *Muon anomalous magnetic moment with staggered fermions: is the lattice spacing small enough?*, *Phys. Rev. D* **106** (2022) 054503 [arXiv:2204.12256] [INSPIRE].

[95] RBC and UKQCD collaborations, *Update of Euclidean windows of the hadronic vacuum polarization*, *Phys. Rev. D* **108** (2023) 054507 [arXiv:2301.08696] [INSPIRE].

[96] FERMILAB LATTICE et al. collaborations, *Light-quark connected intermediate-window contributions to the muon g-2 hadronic vacuum polarization from lattice QCD*, *Phys. Rev. D* **107** (2023) 114514 [arXiv:2301.08274] [INSPIRE].

[97] M. Davier et al., *The euclidean Adler function and its interplay with $\Delta\alpha_{QED}^{had}$ and α_s*, *JHEP* **04** (2023) 067 [arXiv:2302.01359] [INSPIRE].

[98] CMD-3 collaboration, *Measurement of the $e^+e^- \to \pi^+\pi^-$ cross section from threshold to $1.2\,GeV$ with the CMD-3 detector*, arXiv:2302.08834 [INSPIRE].

[99] G. Benton et al., *Data-driven determination of the light-quark connected component of the intermediate-window contribution to the muon $g − 2$*, arXiv:2306.16808 [INSPIRE].

[100] M. Davier et al., *Hadronic vacuum polarization: comparing lattice QCD and data-driven results in systematically improvable ways*, arXiv:2308.04221 [INSPIRE].

[101] A. Pich, *Precision Tau Physics*, *Prog. Part. Nucl. Phys.* **75** (2014) 41 [arXiv:1310.7922] [INSPIRE].

[102] MEG collaboration, *Search for the lepton flavour violating decay $\mu^+ \to e^+\gamma$ with the full dataset of the MEG experiment*, *Eur. Phys. J. C* **76** (2016) 434 [arXiv:1605.05081] [INSPIRE].

[103] SINDRUM collaboration, *Search for the Decay $\mu^+ \to e^+e^+e^-$*, *Nucl. Phys. B* **299** (1988) 1 [INSPIRE].

[104] SINDRUM II collaboration, *A search for muon to electron conversion in muonic gold*, *Eur. Phys. J. C* **47** (2006) 337 [ɪɴSPIRE].

[105] BaBar collaboration, *Searches for Lepton Flavor Violation in the Decays* $\tau^{\pm} \to e^{\pm}\gamma$ *and* $\tau^{\pm} \to \mu^{\pm}\gamma$, *Phys. Rev. Lett.* **104** (2010) 021802 [arXiv:0908.2381] [ɪɴSPIRE].

[106] K. Hayasaka et al., *Search for Lepton Flavor Violating Tau Decays into Three Leptons with 719 Million Produced Tau+Tau- Pairs*, *Phys. Lett. B* **687** (2010) 139 [arXiv:1001.3221] [ɪɴSPIRE].

[107] Belle collaboration, *Search for lepton flavor violating* τ^{-} *decays into* $\ell^{-}\eta$, $\ell^{-}\eta'$ *and* $\ell^{-}\pi^{0}$, *Phys. Lett. B* **648** (2007) 341 [hep-ex/0703009] [ɪɴSPIRE].

[108] Belle collaboration, *Search for Lepton-Flavor-Violating and Lepton-Number-Violating* $\tau \to \ell h h'$ *Decay Modes*, *Phys. Lett. B* **719** (2013) 346 [arXiv:1206.5595] [ɪɴSPIRE].

[109] Belle collaboration, *Search for lepton-flavor-violating tau-lepton decays to* $\ell\gamma$ *at Belle*, *JHEP* **10** (2021) 19 [arXiv:2103.12994] [ɪɴSPIRE].

[110] BaBar collaboration, *Search for Lepton Flavor Violating Decays* $\tau^{\pm} \to \ell^{\pm}\pi^{0}$, $\ell^{\pm}\eta$, $\ell^{\pm}\eta'$, *Phys. Rev. Lett.* **98** (2007) 061803 [hep-ex/0610067] [ɪɴSPIRE].

[111] S. Davidson et al., *Charged Lepton Flavor Violation*, arXiv:2209.00142 [ɪɴSPIRE].

[112] A. Crivellin, S. Davidson, G.M. Pruna and A. Signer, *Renormalisation-group improved analysis of* $\mu \to e$ *processes in a systematic effective-field-theory approach*, *JHEP* **05** (2017) 117 [arXiv:1702.03020] [ɪɴSPIRE].

[113] MEG II collaboration, *The design of the MEG II experiment*, *Eur. Phys. J. C* **78** (2018) 380 [arXiv:1801.04688] [ɪɴSPIRE].

[114] Mu2e collaboration, *Mu2e Technical Design Report*, arXiv:1501.05241 [DOI:10.2172/1172555] [ɪɴSPIRE].

[115] Mu3e collaboration, *Technical design of the phase I Mu3e experiment*, *Nucl. Instrum. Meth. A* **1014** (2021) 165679 [arXiv:2009.11690] [ɪɴSPIRE].

[116] A. Celis, V. Cirigliano and E. Passemar, *Model-discriminating power of lepton flavor violating* τ *decays*, *Phys. Rev. D* **89** (2014) 095014 [arXiv:1403.5781] [ɪɴSPIRE].

[117] V. Cirigliano et al., *Charged Lepton Flavor Violation at the EIC*, *JHEP* **03** (2021) 256 [arXiv:2102.06176] [ɪɴSPIRE].

[118] T. Husek, K. Monsalvez-Pozo and J. Portoles, *Lepton-flavour violation in hadronic tau decays and* $\mu - \tau$ *conversion in nuclei*, *JHEP* **01** (2021) 059 [arXiv:2009.10428] [ɪɴSPIRE].

[119] S. Banerjee et al., *Snowmass 2021 White Paper: charged lepton flavor violation in the tau sector*, arXiv:2203.14919 [ɪɴSPIRE].

[120] Belle-II collaboration, *Snowmass White Paper: Belle II physics reach and plans for the next decade and beyond*, arXiv:2207.06307 [ɪɴSPIRE].

[121] A. Falkowski and D. Straub, *Flavourful SMEFT likelihood for Higgs and electroweak data*, *JHEP* **04** (2020) 066 [arXiv:1911.07866] [ɪɴSPIRE].

[122] A. Efrati, A. Falkowski and Y. Soreq, *Electroweak constraints on flavorful effective theories*, *JHEP* **07** (2015) 018 [arXiv:1503.07872] [ɪɴSPIRE].

[123] P. Janot and S. Jadach, *Improved Bhabha cross section at LEP and the number of light neutrino species*, *Phys. Lett. B* **803** (2020) 135319 [arXiv:1912.02067] [ɪɴSPIRE].

[124] D. Barducci et al., *Interpreting top-quark LHC measurements in the standard-model effective field theory*, `arXiv:1802.07237` [ɪɴSPIRE].

[125] F. Maltoni, L. Mantani and K. Mimasu, *Top-quark electroweak interactions at high energy*, *JHEP* **10** (2019) 004 [`arXiv:1904.05637`] [ɪɴSPIRE].

[126] I. Brivio et al., *O new physics, where art thou? A global search in the top sector*, *JHEP* **02** (2020) 131 [`arXiv:1910.03606`] [ɪɴSPIRE].

[127] G. Durieux et al., *The electro-weak couplings of the top and bottom quarks — Global fit and future prospects*, *JHEP* **12** (2019) 98 [*Erratum ibid.* **01** (2021) 195] [`arXiv:1907.10619`] [ɪɴSPIRE].

[128] N.P. Hartland et al., *A Monte Carlo global analysis of the Standard Model Effective Field Theory: the top quark sector*, *JHEP* **04** (2019) 100 [`arXiv:1901.05965`] [ɪɴSPIRE].

[129] S. Bruggisser, R. Schäfer, D. van Dyk and S. Westhoff, *The Flavor of UV Physics*, *JHEP* **05** (2021) 257 [`arXiv:2101.07273`] [ɪɴSPIRE].

[130] SMEFɪT collaboration, *Combined SMEFT interpretation of Higgs, diboson, and top quark data from the LHC*, *JHEP* **11** (2021) 089 [`arXiv:2105.00006`] [ɪɴSPIRE].

[131] V. Miralles et al., *The top quark electro-weak couplings after LHC Run 2*, *JHEP* **02** (2022) 032 [`arXiv:2107.13917`] [ɪɴSPIRE].

[132] G. Durieux et al., *Snowmass White Paper: prospects for the measurement of top-quark couplings*, in the proceedings of the *Snowmass 2021*, Seattle, U.S.A., July 17–26 (2022) [`arXiv:2205.02140`] [ɪɴSPIRE].

[133] J. de Blas et al., *Global SMEFT Fits at Future Colliders*, in the proceedings of the *Snowmass 2021*, Seattle, U.S.A., July 17–26 (2022) [`arXiv:2206.08326`] [ɪɴSPIRE].

[134] S. Bruggisser, D. van Dyk and S. Westhoff, *Resolving the flavor structure in the MFV-SMEFT*, *JHEP* **02** (2023) 225 [`arXiv:2212.02532`] [ɪɴSPIRE].

[135] T. Giani, G. Magni and J. Rojo, *SMEFiT: a flexible toolbox for global interpretations of particle physics data with effective field theories*, *Eur. Phys. J. C* **83** (2023) 393 [`arXiv:2302.06660`] [ɪɴSPIRE].

[136] Z. Kassabov et al., *The top quark legacy of the LHC Run II for PDF and SMEFT analyses*, *JHEP* **05** (2023) 205 [`arXiv:2303.06159`] [ɪɴSPIRE].

[137] C. Grunwald, G. Hiller, K. Kröninger and L. Nollen, *More synergies from beauty, top, Z and Drell-Yan measurements in SMEFT*, *JHEP* **11** (2023) 110 [`arXiv:2304.12837`] [ɪɴSPIRE].

[138] B.M. Gavela, E.E. Jenkins, A.V. Manohar and L. Merlo, *Analysis of General Power Counting Rules in Effective Field Theory*, *Eur. Phys. J. C* **76** (2016) 485 [`arXiv:1601.07551`] [ɪɴSPIRE].

[139] I. Doršner et al., *Physics of leptoquarks in precision experiments and at particle colliders*, *Phys. Rept.* **641** (2016) 1 [`arXiv:1603.04993`] [ɪɴSPIRE].

[140] J. de Blas, J.C. Criado, M. Perez-Victoria and J. Santiago, *Effective description of general extensions of the Standard Model: the complete tree-level dictionary*, *JHEP* **03** (2018) 109 [`arXiv:1711.10391`] [ɪɴSPIRE].

[141] P. Arnan, D. Becirevic, F. Mescia and O. Sumensari, *Probing low energy scalar leptoquarks by the leptonic W and Z couplings*, *JHEP* **02** (2019) 109 [`arXiv:1901.06315`] [ɪɴSPIRE].

[142] A. Crivellin, D. Müller and F. Saturnino, *Flavor Phenomenology of the Leptoquark Singlet-Triplet Model*, *JHEP* **06** (2020) 020 [arXiv:1912.04224] [INSPIRE].

[143] S. Saad, *Combined explanations of* $(g-2)_\mu$, $R_{D^{(*)}}$, $R_{K^{(*)}}$ *anomalies in a two-loop radiative neutrino mass model*, *Phys. Rev. D* **102** (2020) 015019 [arXiv:2005.04352] [INSPIRE].

[144] A. Crivellin, D. Müller and F. Saturnino, *Leptoquarks in oblique corrections and Higgs signal strength: status and prospects*, *JHEP* **11** (2020) 094 [arXiv:2006.10758] [INSPIRE].

[145] V. Gherardi, D. Marzocca and E. Venturini, *Low-energy phenomenology of scalar leptoquarks at one-loop accuracy*, *JHEP* **01** (2021) 138 [arXiv:2008.09548] [INSPIRE].

[146] D. Marzocca, S. Trifinopoulos and E. Venturini, *From B-meson anomalies to Kaon physics with scalar leptoquarks*, *Eur. Phys. J. C* **82** (2022) 320 [arXiv:2106.15630] [INSPIRE].

[147] V. Gherardi, D. Marzocca and E. Venturini, *Matching scalar leptoquarks to the SMEFT at one loop*, *JHEP* **07** (2020) 225 [*Erratum ibid.* **01** (2021) 006] [arXiv:2003.12525] [INSPIRE].

[148] ATLAS collaboration, *Search for new phenomena in pp collisions in final states with tau leptons, b-jets, and missing transverse momentum with the ATLAS detector*, *Phys. Rev. D* **104** (2021) 112005 [arXiv:2108.07665] [INSPIRE].

[149] B. Belfatto, R. Beradze and Z. Berezhiani, *The CKM unitarity problem: a trace of new physics at the TeV scale?*, *Eur. Phys. J. C* **80** (2020) 149 [arXiv:1906.02714] [INSPIRE].

[150] V. Cirigliano et al., *Beta-decay implications for the W-boson mass anomaly*, *Phys. Rev. D* **106** (2022) 075001 [arXiv:2204.08440] [INSPIRE].

[151] A. Crivellin, *Explaining the Cabibbo Angle Anomaly*, arXiv:2207.02507 [INSPIRE].

[152] A.J. Buras, J. Girrbach-Noe, C. Niehoff and D.M. Straub, $B \to K^{(*)}\nu\bar{\nu}$ *decays in the Standard Model and beyond*, *JHEP* **02** (2015) 184 [arXiv:1409.4557] [INSPIRE].

[153] D. Bečirević, O. Sumensari and R. Zukanovich Funchal, *Lepton flavor violation in exclusive* $b \to s$ *decays*, *Eur. Phys. J. C* **76** (2016) 134 [arXiv:1602.00881] [INSPIRE].

[154] K. De Bruyn et al., *Branching Ratio Measurements of* B_s *Decays*, *Phys. Rev. D* **86** (2012) 014027 [arXiv:1204.1735] [INSPIRE].

[155] K. De Bruyn et al., *Probing New Physics via the* $B_s^0 \to \mu^+\mu^-$ *Effective Lifetime*, *Phys. Rev. Lett.* **109** (2012) 041801 [arXiv:1204.1737] [INSPIRE].

[156] S. Aoki et al., *Review of lattice results concerning low-energy particle physics*, *Eur. Phys. J. C* **77** (2017) 112 [arXiv:1607.00299] [INSPIRE].

[157] G. Hiller and M. Schmaltz, *Diagnosing lepton-nonuniversality in* $b \to s\ell\ell$, *JHEP* **02** (2015) 055 [arXiv:1411.4773] [INSPIRE].

[158] M. Ciuchini et al., *New Physics in* $b \to s\ell^+\ell^-$ *confronts new data on Lepton Universality*, *Eur. Phys. J. C* **79** (2019) 719 [arXiv:1903.09632] [INSPIRE].

[159] G. Hiller and I. Nisandzic, R_K *and* R_{K^*} *beyond the standard model*, *Phys. Rev. D* **96** (2017) 035003 [arXiv:1704.05444] [INSPIRE].

[160] L.-S. Geng et al., *Towards the discovery of new physics with lepton-universality ratios of* $b \to s\ell\ell$ *decays*, *Phys. Rev. D* **96** (2017) 093006 [arXiv:1704.05446] [INSPIRE].

[161] W. Altmannshofer et al., *Symmetries and Asymmetries of* $B \to K^*\mu^+\mu^-$ *Decays in the Standard Model and Beyond*, *JHEP* **01** (2009) 019 [arXiv:0811.1214] [INSPIRE].

[162] A. Bharucha, D.M. Straub and R. Zwicky, $B \to V\ell^+\ell^-$ *in the Standard Model from light-cone sum rules*, *JHEP* **08** (2016) 098 [arXiv:1503.05534] [INSPIRE].

[163] J. Aebischer, A.J. Buras and J. Kumar, *On the Importance of Rare Kaon Decays: a Snowmass 2021 White Paper*, in the proceedings of the *Snowmass 2021*, Seattle, U.S.A., July 17–26 (2022) [arXiv:2203.09524] [INSPIRE].

[164] A. Angelescu, D.A. Faroughy and O. Sumensari, *Lepton Flavor Violation and Dilepton Tails at the LHC*, *Eur. Phys. J. C* **80** (2020) 641 [arXiv:2002.05684] [INSPIRE].

[165] M. Misiak et al., *Updated NNLO QCD predictions for the weak radiative B-meson decays*, *Phys. Rev. Lett.* **114** (2015) 221801 [arXiv:1503.01789] [INSPIRE].

[166] M. Czakon et al., *The* $(Q_7, Q_{1,2})$ *contribution to* $\overline{B} \to X_s\gamma$ *at* $\mathcal{O}\left(\alpha_s^2\right)$, *JHEP* **04** (2015) 168 [arXiv:1503.01791] [INSPIRE].

[167] W. Dekens, E.E. Jenkins, A.V. Manohar and P. Stoffer, *Non-perturbative effects in* $\mu \to e\gamma$, *JHEP* **01** (2019) 088 [arXiv:1810.05675] [INSPIRE].

[168] M. González-Alonso, J. Martin Camalich and K. Mimouni, *Renormalization-group evolution of new physics contributions to (semi)leptonic meson decays*, *Phys. Lett. B* **772** (2017) 777 [arXiv:1706.00410] [INSPIRE].